

Allele-Specific Silencing of Mutant mRNA Rescues Ultrastructural and Arrhythmic Phenotype in Mice Carriers of the R4496C Mutation in the Ryanodine Receptor Gene (*RYR2*)

Rossana Bongianino, Marco Denegri, Andrea Mazzanti, Francesco Lodola, Alessandra Vollero, Simona Boncompagni, Silvia Fasciano, Giulia Rizzo, Damiano Mangione, Serena Barbaro, Alessia Di Fonso, Carlo Napolitano, Alberto Auricchio, Feliciano Protasi, Silvia G. Priori

Rationale: Mutations in the cardiac Ryanodine Receptor gene (*RYR2*) cause dominant catecholaminergic polymorphic ventricular tachycardia (CPVT), a leading cause of sudden death in apparently healthy individuals exposed to emotions or physical exercise.

Objective: We investigated the efficacy of allele-specific silencing by RNA interference to prevent CPVT phenotypic manifestations in our dominant CPVT mice model carriers of the heterozygous mutation R4496C in *RYR2*.

Methods and Results: We developed an in vitro mRNA and protein-based assays to screen multiple siRNAs for their ability to selectively silence mutant *RYR2*-R4496C mRNA over the corresponding wild-type allele. For the most performant of these siRNAs (siRYR2-U10), we evaluated the efficacy of an adeno-associated serotype 9 viral vector (AAV9) expressing miRYR2-U10 in correcting RyR2 (Ryanodine Receptor type 2 protein) function after in vivo delivery by intraperitoneal injection in neonatal and adult RyR2^{R4496C/+} (mice heterozygous for the R4496C mutation in the RyR2) heterozygous CPVT mice. Transcriptional analysis showed that after treatment with miRYR2-U10, the ratio between wild-type and mutant *RYR2* mRNA was doubled (from 1:1 to 2:1) confirming the ability of miRYR2-U10 to selectively inhibit *RYR2*-R4496C mRNA, whereas protein quantification showed that total RyR2 was reduced by 15% in the heart of treated mice. Furthermore, AAV9-miRYR2-U10 effectively (1) reduced isoproterenol-induced delayed afterdepolarizations and triggered activity in infected cells, (2) reduced adrenergically mediated ventricular tachycardia in treated mice, (3) reverted ultrastructural abnormalities of junctional sarcoplasmic reticulum and transverse tubules, and (4) attenuated mitochondrial abnormalities.

Conclusions: The study demonstrates that allele-specific silencing with miRYR2-U10 prevents life-threatening arrhythmias in CPVT mice, suggesting that the reduction of mutant RyR2 may be a novel therapeutic approach for CPVT. (*Circ Res.* 2017;121:525-536. DOI: 10.1161/CIRCRESAHA.117.310882.)

Key Words: cardiac arrhythmia ■ cardiac sudden death ■ catecholaminergic polymorphic ventricular tachycardia ■ gene therapy ■ genetics ■ Ryanodine receptor calcium channel ■ transgenic mice

Catecholaminergic polymorphic ventricular tachycardia (CPVT) is a genetic disease characterized by stress-induced life-threatening arrhythmias occurring in otherwise healthy individuals. CPVT usually manifests in early childhood with unexplained syncopal spells in patients with normal heart.¹

Editorial, see p 480
Meet the First Author, see p 470

Dominant CPVT is caused by mutations in the Ryanodine Receptor (*RYR2*) gene² that encodes a large 560 KDa protein that forms a homotetrameric ion channel localized in the membrane of the junctional sarcoplasmic reticulum (jSR). RyR2 (Ryanodine Receptor type 2 protein) channels face the L-type Ca²⁺ channels (Cav1.2), which are positioned in specialized invaginations of the cellular membrane called transverse tubules (TT): influx of Ca²⁺ through these channels

Original received February 22, 2017; revision received June 7, 2017; accepted June 14, 2017. In May 2017, the average time from submission to first decision for all original research papers submitted to *Circulation Research* was 12.28 days.

From the Molecular Cardiology, IRCCS Istituti Clinici Scientifici Maugeri, Pavia, Italy (R.B., A.M., F.L., A.V., S.F., G.R., D.M., S.B., C.N., S.G.P.); Department of Molecular Medicine, University of Pavia, Italy (R.B., A.M., S.F., S.G.P.); CeSI-Met - Center for Research on Ageing and Translational Medicine & DNICS - Department of Neuroscience, Imaging and Clinical Sciences, University G. d'Annunzio, Chieti, Italy (S.B., A.D.F.); CeSI-Met - Center for Research on Ageing and Translational Medicine and DMSI, Department of Medicine and Aging Sciences, University G. d'Annunzio, Chieti, Italy (F.P.); Telethon Institute of Genetics and Medicine, Naples, Italy (A.A.); and Medical Genetics, Department of Translational Medicine, Federico II University, Naples, Italy (A.A.).

This manuscript was sent to Masao Endoh, Consulting Editor, for review by expert referees, editorial decision, and final disposition.

The online-only Data Supplement is available with this article at <http://circres.ahajournals.org/lookup/suppl/doi:10.1161/CIRCRESAHA.117.310882/-/DC1>.

Correspondence to Silvia G. Priori, MD, PhD, Division of Cardiology and Molecular Cardiology, Istituti Clinici Scientifici Maugeri, IRCCS, Via Maugeri 10/10A, 27100 Pavia, Italy. E-mail silvia.priori@icsmaugeri.it

© 2017 American Heart Association, Inc.

Circulation Research is available at <http://circres.ahajournals.org>

DOI: 10.1161/CIRCRESAHA.117.310882

Novelty and Significance

What Is Known?

- RyR2 (Ryanodine Receptor type 2 protein) release Ca^{2+} from the sarcoplasmic reticulum during excitation–contraction coupling.
- Mutations in Ryanodine Receptor (*RYR2*) gene cause catecholaminergic polymorphic ventricular tachycardia (CPVT).
- In *RYR2* mutant cardiac myocytes, adrenergic stimulation elicits diastolic Ca^{2+} release causing triggered activity and life-threatening arrhythmias.

What New Information Does This Article Contribute?

- Specific inhibition of the mutant allele of *RYR2* by adeno-associated virus–mediated RNA interference dramatically reduces arrhythmias in $\text{RyR2}^{\text{R4496C/+}}$ (mice heterozygous for the R4496C mutation in the Ryanodine Receptor 2 gene) knock-in mice exposed to adrenergic stimulation and suppresses triggered activity in infected cardiac myocytes.
- Ultrastructural abnormalities of junctional sarcoplasmic reticulum and mitochondria are present in the heart of $\text{RyR2}^{\text{R4496C/+}}$ CPVT mice.
- Allele-specific targeted RNA interference substantially reduces ultrastructural abnormalities, suggesting that diastolic calcium release may promote mitochondria and sarcoplasmic reticulum alterations.

CPVT is an inherited arrhythmic disorder linked to mutations in the cardiac *RYR2* gene. Current therapies provide an incomplete protection from sudden death; thus, the search for a therapeutic approach to revert molecular and functional abnormalities of the disease is a priority. In this study, we show that in a mouse model of CPVT specific inhibition of mutant *RYR2* expression by viral vector-mediated RNA interference decreased the incidence of adrenergic induced ventricular arrhythmias in vitro and in vivo. Phenotypic rescue derives from the suppression of triggered action potentials that is observed in transduced cardiac myocytes of treated animals. Transcriptional analysis demonstrates that such antiarrhythmic efficacy parallels the predicted reduction of mutant versus wild-type subunits, suggesting that the ratio between wild-type and mutant RyR2 may be a determinant of the severity of clinical manifestations. Furthermore, we found that cardiac myocytes of CPVT mice present ultrastructural abnormalities of mitochondria and calcium release units that are mainly recovered by the mutant allele-specific silencing therapy. These data provide the proof of concept that selective inhibition of mutant *RYR2* allele may evolve into a therapeutic strategy for CPVT patients.

Nonstandard Abbreviations and Acronyms

AAV9	adeno-associated virus serotype 9
CASQ2	calsequestrin 2
CPVT	catecholaminergic polymorphic ventricular tachycardia
CRU	calcium release unit
DADs	delayed afterdepolarizations
GC	Genome Copies
GFP	green fluorescent protein
Het	heterozygous $\text{RyR2}^{\text{R4496C/+}}$
Het-SCR	heterozygous $\text{RyR2}^{\text{R4496C/+}}$ infected with AAV9-miRNA-Scramble
Het-U10	heterozygous $\text{RyR2}^{\text{R4496C/+}}$ infected with AAV9-miR2-U10
jSR	junctional sarcoplasmic reticulum
miRNA	microRNA
PCR	polymerase chain reaction
RYR2	Ryanodine Receptor type 2 gene
RyR2	Ryanodine Receptor type 2 protein
$\text{RyR2}^{\text{R4496C/+}}$	mice heterozygous for the R4496C mutation in the Ryanodine Receptor 2 gene
SR	sarcoplasmic reticulum
TA	triggered activity
TT	transverse tubules
WT	wild type

triggers RyR2-mediated Ca^{2+} release from the sarcoplasmic reticulum (SR), eliciting contraction of the heart.³

In normal myocytes, sympathetic activation promotes phosphorylation of RyR2 and increases Ca^{2+} release from the SR, whereas, in the presence of *RYR2* gain-of-function mutations, in addition to the physiological response, adrenergic activation also elicits spontaneous diastolic Ca^{2+} release. In response to the increase in cytosolic Ca^{2+} , the $\text{Na}^+/\text{Ca}^{2+}$ exchanger extrudes

1 Ca^{2+} ion for 3 Na^+ ions: this electrogenic stoichiometry generates delayed afterdepolarizations (DADs) that depolarize cardiac cells and precipitate triggered arrhythmias.⁴

The first-line therapy to prevent adrenergically mediated arrhythmias in CPVT is β -blockers. However, follow-up data in different populations^{2,5} showed recurrence of arrhythmic events in about 25% of patients, thus highlighting the incomplete protection of this treatment. Patients who show recurrent arrhythmias on β -blockers are treated with flecainide. In high-risk patients with arrhythmic outbreaks despite optimal medical therapy, the implant of a defibrillator is recommended.⁶ The burden of life-long treatment with partially effective drugs and the complications related to the implant of a defibrillator in young patients poses the rationale for the development of more effective therapeutic approaches for CPVT.

We previously demonstrated that adeno-associated virus (AAV)–mediated delivery of the cDNA of the wild-type (WT) sequence of the Calsequestrin 2 (*CASQ2*) gene to knock-in mice affected by the recessive form of CPVT is highly effective in preventing life-threatening arrhythmias.⁷ Our data also showed that AAV-mediated delivery of WT cDNA of *CASQ2* reverts all the biomarkers of the disease such as reduction of levels of *CASQ2*, triadin, and junctin, the abnormal intracellular calcium physiology, and the ultrastructural abnormalities of the jSR and the TT.⁷ In the attempt to devise a gene therapy strategy for the dominant form of CPVT, we hypothesized that the silencing of the mutant allele of the *RYR2* gene using RNA interference could represent a viable strategy to test in our $\text{RyR2}^{\text{R4496C/+}}$ (mice heterozygous for the R4496C mutation in the Ryanodine Receptor 2 gene) heterozygous CPVT mice that we extensively characterized in the past 10 years.^{8–10} This approach has to face several possible challenges because it is unpredictable whether it will be possible to obtain in vivo a highly selective silencing of the mutant allele devoid of silencing of

the WT protein. Furthermore, it is uncertain whether RNA interference will be able to reduce a significant amount of the mutant protein sufficient to reduce the arrhythmic burden.

Methods

For a more detailed description of Methods, the readers are encouraged to access the [Online Data Supplement](#).

Cloning of Reporter Alleles, siRNA Design, and Selection

We developed an in vitro mRNA and protein-based assay suitable to screen multiple siRNAs designed to selectively target the murine R4496C mutant allele over the WT *RYR2* allele. We used 2 mini-constructs containing the WT and the mutant portion of the *RYR2* gene encompassing exons 91 to 96 linked with a protein tag and a fluorescent reporter gene (Online Figure IA) to screen a set of siRNA duplexes. These were modeled on the murine *RYR2* mRNA sequence spanning the R4496C point mutation site and differing for the position of the mutation recognition site, the key parameter that determines the thermodynamic properties of the pairing between the siRNA and the target mRNA and influences the specificity of the silencing activity (Online Figure IB). Heterozygous conditions were generated by cotransfecting the 2 reporter alleles and siRNA duplexes into cultured HEK-293 (human embryonic kidney cells 293) cells.

Among the tested molecules designed to target *RYR2* mRNA containing the R4496C mutation, we selected siRYR2-U10 siRNA duplex sequence (siRYR2: siRNA targeted to *RYR2* sequence), meaning that the mutation recognition site is in position 10 of the sense strand, as the most selective molecule able to reduce R4496C-*RYR2* mRNA without inducing significant knockdown of the corresponding WT mRNA.

By ligation of annealed oligonucleotides, siRYR2-U10 was cloned into a commercially available artificial microRNA (miRNA) expression vector (BLOCK-iT Pol II miR RNAi Expression vector; Life Technologies) that allows the continuous and long-term transcription of the silencing molecule by a cytomegalovirus (CMV) promoter and the coexpression with the GFP (green fluorescent protein) reporter gene.

Subsequently, we transferred the CMV-miRYR2-U10-GFP cassette (miRYR2: miRNA targeted to *RYR2* sequence) and a similar cassette encoding a scramble miRNA, unable to target any known vertebrate gene, into an AAV backbone plasmid (pAAV2.1_CMV-GFP-miRYR2-U10-TkpolyA and pAAV2.1_CMV-GFP-miRNA-Scramble-TkpolyA). We will refer to the 2 viral constructs as AAV9-miRYR2-U10 and AAV9-miRNA-Scramble (Online Figure II). The AAV production was performed at the Tigem Institute (<http://www.tigem.it/core-facilities/vector-core>).

Cell Culture and Transfection

HEK-293 cells were cultured in Dulbecco modified Eagle medium supplemented with 10% fetal bovine serum and 1% penicillin/streptomycin, 1% of L-glutamine, 1 mmol/L sodium pyruvate, and 1% nonessential amino acid solution at 37°C in 5% CO₂. Lipofectamine 2000 (Life Technologies) was used for transient transfection according to the manufacturer's protocol. siRNAs were diluted in OptiMEM together with pGFP_RYR2ex91-96/R4496C_3xFLAG and pRFP_RYR2ex91-96/WT_3xHA. siRNA final concentration was 50 nmol/L unless otherwise indicated. Analyses were performed after 48 hours.

RNA Extraction, Retrotranscription, and Real-Time Polymerase Chain Reaction

HEK-293 cells transiently transfected with equal amount of the reporter alleles and RNAi molecules were lysed, and total RNA was purified with RNeasy mini kit (Qiagen). RNeasy Fibrous Tissue mini kit (Qiagen) was used for RNA extraction from isolated hearts and other organs derived from infected and control mice. A total amount of 1 µg template RNA per reaction was used for a 20 µL retrotranscription, performed with iScript cDNA Synthesis kit (Bio-Rad) according to the manufacturer's instruction.

Protein Extraction and Immunoblotting

Protein expression analysis was performed using the following antibodies: anti-FLAG (F3165; Sigma-Aldrich), anti-HA (H3663; Sigma-Aldrich), anti-RyR2 (MA3-916; Thermo Scientific). Pan Cadherin was used as reference protein using an anti-Pan Cadherin antibody (C1821; Sigma-Aldrich). As secondary antibody we used a horseradish peroxidase-conjugated antimouse antibody (W402B; Promega). Immunoblotting membranes were revealed using the Clarity Western ECL substrate (Bio-Rad) and detected using ChemiDoc MP Imaging System (Bio-Rad). Quantification of protein expression has been performed by densitometry normalization on the reference protein Pan Cadherin with Image Laboratory Software (Bio-Rad).

EKG Monitoring, Echocardiography, and Drug Testing

All animal studies were conducted in compliance of institutional guidelines and according to the Committee for animal well-being of the University of Pavia. Animal studies were approved by the Italian Ministry of Health (Approval no. 879/2015-PR). In this study, we used Het (heterozygous RyR2^{R4496C/+}) knock-in mice (patent US7741529 B1) previously characterized in our laboratory.⁸⁻¹⁰ In vivo studies were performed delivering miRYR2-U10 and the miRNA-Scramble packaged in an AAV serotype 9 (AAV9) which was selected for its cardiac tropism.¹¹ We injected intraperitoneally 1.3×10¹² AAV9 viral particles in neonates at day 8 and 3.9×10¹² AAV9 viral particles at day 30 (p30) after birth in Het. A dose-response curve was performed in Het mice injecting 1×10¹² AAV9, 2×10¹² AAV9, and 3×10¹² AAV9 viral p30 after birth to identify the threshold for the antiarrhythmic efficacy. Animals were euthanized after 8 weeks, and cardiac myocytes were isolated for characterization. Fluorescence microscopy imaging of RyR2^{R4496C/+} myocytes from infected hearts showed a transduction rate of about 80±5% in mice infected at particles at day 8 (Online Figure IIIA and IIIB) and of about 66±12% in mice infected at p30; the cardiospecificity of transduction was confirmed by real-time polymerase chain reaction (PCR) comparing GFP expression in different organs (Online Figure IIIC).

EKG recording was performed using subcutaneous implantable EKG transmitters with the DSI PhysioTel Implantable Telemetry system (Data Sciences International). Baseline EKGs were recorded for 10 minutes in resting conditions in conscious animals followed by intraperitoneal delivery of 2 mg/kg epinephrine and 120 mg/kg caffeine injection and observation for additional 15 minutes. Quantification of arrhythmic episodes was performed offline by 2 blinded investigators. Echocardiography was performed at 8 weeks in mice sedated with isoflurane 1% with a Visual Sonics Vevo 2100 Ultrasound (Visual Sonics Inc) equipment using a 40-MHz linear array transducer. M-mode tracings in parasternal long-axis view were used to measure end-diastolic ventricular diameter and ejection fraction with Teicholz formula.

Action Potential Recordings in Isolated Ventricular Myocytes

Ventricular myocytes from Het, Het-SCR (heterozygous RyR2^{R4496C/+} infected with AAV9-miRNA-Scramble), and Het-U10 (heterozygous RyR2^{R4496C/+} infected with AAV9-miRYR2-U10) mice were isolated with the Langendorff method, using retrograde perfusion through the aorta with enzyme-containing solutions as previously described.^{4,7}

Freshly isolated myocytes were kept in a plastic well surrounded by a heating ring to maintain the perfusion solution at 37°C. Action potentials were recorded with borosilicate glass pipettes with a resistance of 1 to 3 MΩ using the whole-cell patch-clamp technique in the current-clamp mode. Isoproterenol (30 nmol/L) was administered to elicit DADs and triggered activity (TA). Data were analyzed offline with pCLAMP 9.2 (Molecular devices).

Allele-Specific Real-Time PCR

Samples obtained from Het, Het-SCR, and Het-U10 mice were evaluated for *RYR2* allelic expression using quantitative real-time PCR and allele-specific TaqMan probes (Applied Biosystems). RNA extraction and retrotranscription were performed as described

above. All reactions were performed using an Applied Biosystems ViiA7 Real-Time PCR System (Applied Biosystems). A standard curve constructed by mixing the normal and mutant cDNA samples at known ratios and fitted with the equation $\log_2(\text{WT: R4496C ratio}) = \alpha \Delta C_T + \beta$ (α and β are fit parameters) was used to interpolate the ratio of allele expression of samples of animals infected with different doses of viral particles containing miR2-10 and of control samples.

Immunofluorescence on Heart Sections

Cryosections of heart tissue were prepared for immunofluorescence performed with the following antibodies: anti- α -actinin (A7811; Sigma-Aldrich), anti-GFP 488-conjugated (600-141-215; Rockland) or Alexa Fluor 594-conjugated goat antimouse secondary antibodies

(A31624; Life Technologies). Dako mounting medium was applied to all slides. Fluorescence images were obtained with a Leica TCS-SP5 II inverted confocal microscope.

Electron Microscopy and Quantitative Analysis of Electron Microscopy Images

Hearts isolated from WT, Het, Het-SCR, and Het-U10 mice were fixed by retrograde aortic perfusion. Ultrathin sections were cut in a Leica Ultracut R microtome (Leica Microsystems, Austria) using a Diatome diamond knife (Diatome Ltd, Biel, Switzerland) and double stained with uranyl acetate and lead citrate. All sections were examined with an FP 505 Morgagni Series 268D electron microscope (FEI Company, Brno, Czech Republic), equipped with Megaview III digital camera and Soft Imaging System (Munster, Germany).

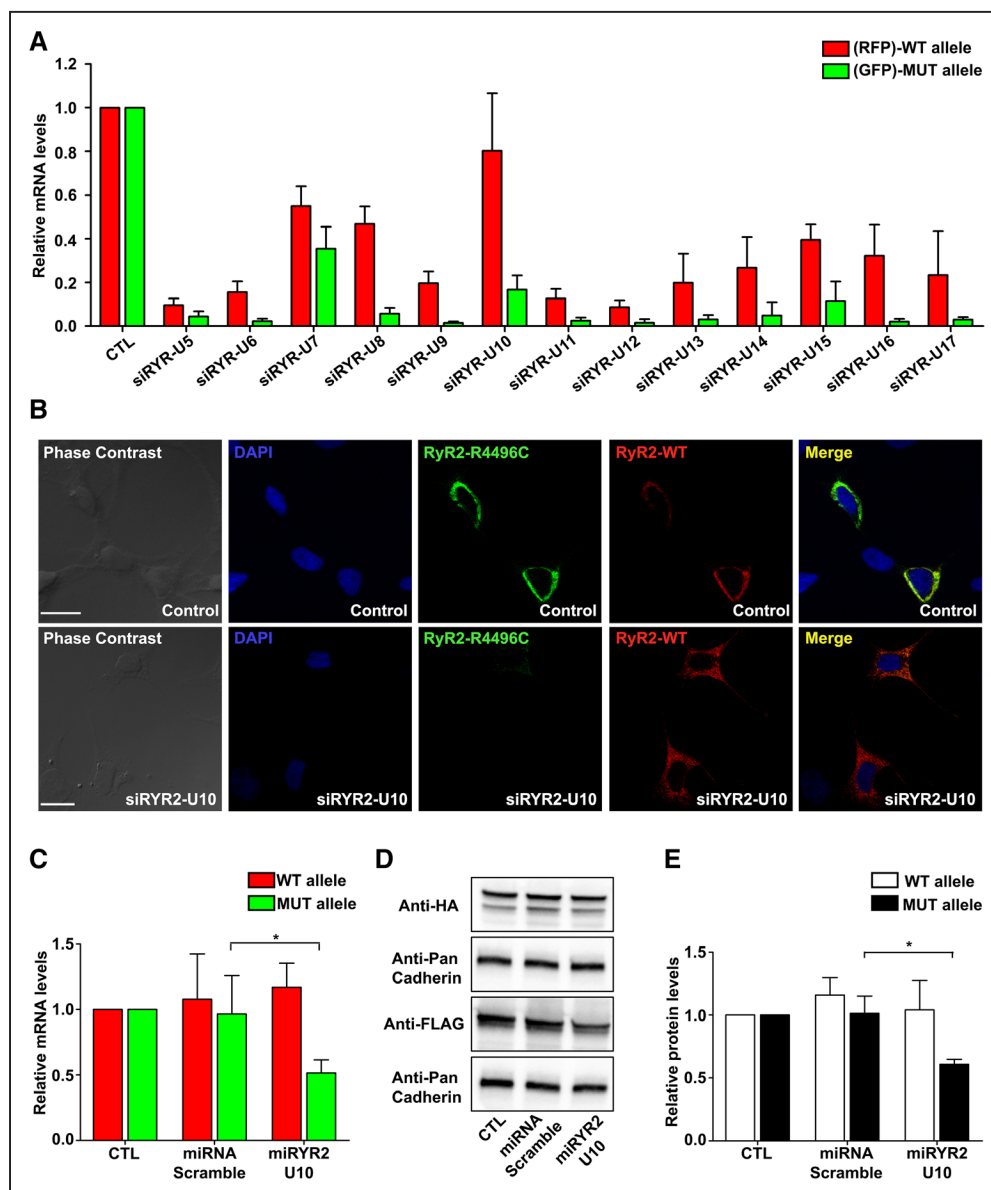


Figure 1. In vitro assessment of mutant Ryanodine Receptor type 2 gene (RYR2)-specific silencing using reporter alleles.

A, Assessment of wild-type (WT; red) and mutant (green) relative mRNA knockdown in HEK-293 cells transiently transfected with reporter alleles and corresponding siRNA ($n=3$ independent experiments). **B**, Fluorescence analysis on HEK-293 (human embryonic kidney cells 293) cells transfected with reporter alleles and the selected siR2-U10 compared with control cells; Scale bars=20 μ m. **C**, Assessment of WT (red) and mutant (green) relative mRNA knockdown in HEK-293 transfected with reporter alleles and pAAV2.1_miR2-U10 ($n=5$) or pAAV2.1_miRNA-Scramble ($n=5$) normalized to levels observed in cells transfected only with the reporter alleles (negative control [CTL]; $n=4$; $*P<0.005$). **D** and **E**, Assessment of WT and mutant protein expression by Western blot in HEK-293 transfected with reporter alleles and pAAV2.1_miR2-U10 ($n=5$) or pAAV2.1_miRNA-Scramble ($n=5$) normalized to levels observed in cells transfected only with reporter alleles (CTL; $n=3$; $*P<0.05$).

The percentage of cardiac cells exhibiting severe structural alterations was quantified. Measurements of relevant parameters of jSR, TT, and mitochondria were performed applying the stereology point-counting technique^{12,13} in micrographs taken at 22,000 of magnification from cross-sections of papillary cardiac myocytes (Online Figure IV). In the assessment of the efficacy of gene therapy in reverting ultrastructural abnormalities in calcium release units (CRUs) and mitochondria, we used the following definitions: we defined as fully recovered those changes induced by therapy with AAV9-miR2-U10 that induce a statistically significant difference in the monitored parameters between Het and Het-U10, while also showing no statistically significant differences in the comparison between WT and Het-U10, thus confirming the return to normal values. We defined as partially recovered those changes induced by therapy with AAV9-miR2-U10 that document a statistically significant difference in the monitored parameters between Het and Het-U10; however, they do not show normalization because data present a statistically significant difference between WT and Het-U10.

Statistical Analysis

Analyses were performed with SPSS Version 21.0 (IBM Corp, Armonk, NY) and GraphPad Prism (version 6.00 for Windows; La Jolla, CA). Sample sizes were calculated on the basis of published studies on the same animal model.⁸ Data are reported as mean±SD or percentage. Continuous variables were compared by ANOVA with Tukey–Kramer post hoc test or Mann–Whitney test, as appropriate. Categorical variables were compared with cross-tabulation applying the Fisher–Freeman–Halton exact test when >2 groups were compared. This was followed by pairwise comparisons with the Fisher exact test with Bonferroni correction. The probabilities of the formation of tetramers with different compositions in Figure 3 were modeled using binomial distribution. The probabilities of forming different tetramers are calculated from the mutant (dark grey)/WT (light grey) ratio.¹⁴ All tests were 2-tailed. *P* values <0.05 were considered significant unless Bonferroni correction was used.

Results

Identification of the siRNA Sequence Suitable for Targeted Silencing of the R4496C-RYR2 Allele

We tested 13 siRNA duplexes in an in vitro assay for their ability to silence the mutant *RYR2* mRNA over the corresponding WT allele. Real-time data showed that the siR2-U10 reduced R4496C-*RYR2* mRNA by 80% without significantly affecting levels of WT mRNA (Figure 1A). Silencing of mutant *RYR2* was confirmed by fluorescence microscopy taking advantage of the fluorescent tags in the reporter alleles (Figure 1B). We then evaluated, in the same in vitro system, the specificity and efficacy of a viral vector plasmid expressing an artificial miRNA, designed to replicate, when transcribed, sense and antisense strands of siR2-U10 cassette under a CMV promoter and linked to a *GFP* reporter gene. The miR2-U10 molecule induced about 50% reduction of the expression of R4496C allele both at the mRNA (Figure 1C; **P*<0.05) and the protein level (Figure 1D and 1E; **P*<0.05) without affecting WT expression.

Analysis of the Effect of miR2-U10 and miRNA-Scramble on levels of RYR2 Transcripts and RyR2 Protein After In Vivo Administration

We quantified the ratio of WT:R4496C-*RYR2* mRNA transcripts from the heart of mice infected with either the AAV9-miRNA-Scramble (Het-SCR) or the AAV9-miRNA-U10 (Het-U10) particles at 8 or 30 days after birth. Transcript analysis showed that in both group of animals, the ratio between WT and mutant

RYR2 transcripts changes from 1:1 seen in untreated heterozygous (Het) and Het-SCR mice and increases to 2:1 in both groups of mice treated at the dose of 3.9×10^{12} AAV9 (Figure 2A and 2B), whereas total *RYR2* mRNA showed no significant changes among groups (Figure 2C and 2D).

Interestingly, the dose–response curve of the AAV9-miR2-U10 (1×10^{12} Genome Copies [GC], 2×10^{12} GC, and 3×10^{12} GC) showed a linear increase of the ratio between WT and mutant transcript at progressively higher dose of the viral construct (Figure 2E).

We therefore modeled the combination of mutant and WT RyR2 monomers to form the tetrameric channel

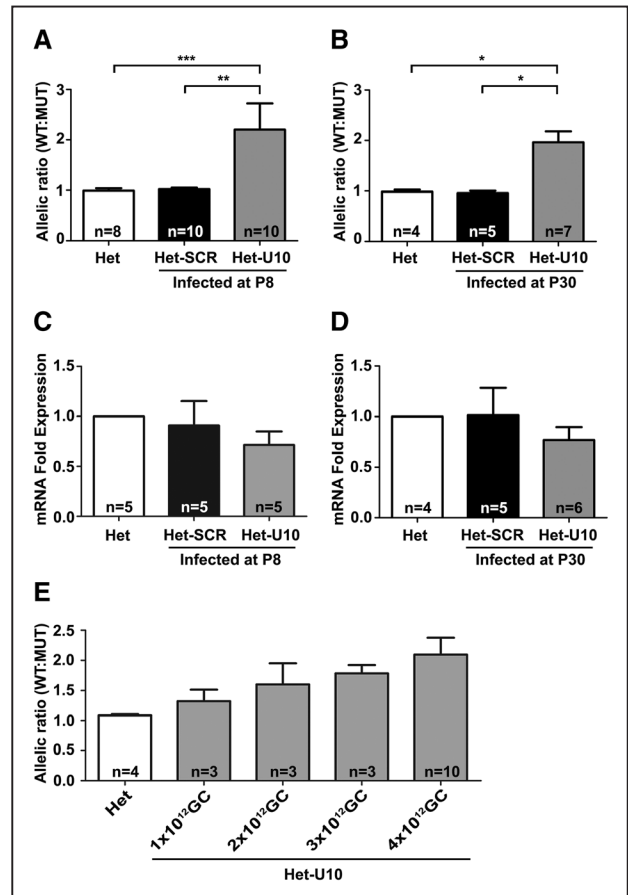


Figure 2. Molecular characterization of RyR2^{R4496C/+} (mice heterozygous for the R4496C mutation in the Ryanodine Receptor 2 gene) mice treated with allele-specific silencing. **A and B.** Quantification of wild-type (WT):R4496C mutant (MUT) mRNA ratio in RyR2^{R4496C/+} untreated mice (Het [heterozygous RyR2^{R4496C/+}]) and in RyR2^{R4496C/+} mice treated at 8 d (p8; **A**) or at 30 d of age (p30; **B**) with either adeno-associated serotype 9 viral vector (AAV9) miR2-U10 (Het-U10 [heterozygous RyR2^{R4496C/+} infected with AAV9-miR2-U10]) or AAV9 miRNA-Scramble (Het-SCR [heterozygous RyR2^{R4496C/+} infected with AAV9-miRNA-Scramble]; **P*<0.05; ***P*<0.005; ****P*<0.001). **C and D.** Quantification of total RYR2 expression in RyR2^{R4496C/+} untreated mice (Het) and in mice treated at 8 d (**C**) and at 30 d of age (**D**) with AAV9 miR2-U10 (Het-U10) or AAV9 miRNA-Scramble (Het-SCR). **E.** Quantification of WT:MUT mRNA ratio in Het-U10 mice injected at p30 with increasing doses of AAV9-miR2-U10 Genome Copies (GC; approximate to single units): 1×10^{12} GC, 2×10^{12} GC, 3×10^{12} GC, and 4×10^{12} GC compared with untreated Het mice. All experiments were performed 2 mo after viral injection. Number of animals per each group is indicated in the bars.

mimicking the setting of untreated Het and Het exposed to AAV9-miR_{YR2} U10 therapy at the dose of 3.9×10^{12} GC assuming random assembly and applying a binomial distribution to assess the impact of mutant mRNA knockdown on the channel. We showed that the change in the ratio between WT and Mutant *RYR2* transcripts enhances the likelihood of completely functional tetramer formation from 6.25% to 19.75% and reduces the probability of totally dysfunctional tetramer formation from 6.25% to 1.23% (Figure 3A). When the combination of WT and mutant RyR2 monomers to form the tetrameric channel was calculated for each of the doses of AAV9-miR_{YR2}-U10 therapy tested, we observed that each increase in the dose corresponded to a linear increase of the percentage of WT monomers and a decrease of the mutant monomers predicted to be incorporated in the RyR2 channels (Figure 3B).

Western blot analysis demonstrated that, when compared with Het mice, the amount of total RyR2 protein was reduced by $\approx 15\%$ in the heart of Het-U10 mice (Online Figure V).

Functional Evaluation of Allele-Specific Silencing in RyR₂^{R4496C/+} Mice-Derived Cardiac Myocytes

Experiments were performed 8 weeks after infection. Patch-clamp experiments were performed to compare the electrophysiological behavior of untreated RyR₂^{R4496C/+} myocytes (Het) exposed to isoproterenol (30 nmol/L) to that of infected

(GFP positive) and noninfected (GFP negative) myocytes isolated from the heart of RyR₂^{R4496C/+} mice infected at day 8 (neonates) with either AAV9-miR_{YR2}-U10 (Het-U10) or AAV9-miRNA-Scramble (Het-SCR). A striking reduction of DADs (Figure 4A and 4B) and TA (Figure 4A and 4C) was observed in GFP-positive cardiac myocytes derived from Het-U10 but not in those from Het-SCR mice or in cells derived from the heart of untreated Het mice.

Similar results were obtained in cells isolated from mice infected with miR_{YR2}-U10 or miRNA-Scramble at day 30 (young adults; Figure 4A, 4D, and 4E). Results of statistical analysis are reported in the legend of Figure 4.

Evaluation of the Incidence of Ventricular Arrhythmias after Allele-Specific Silencing Administration in RyR₂^{R4496C/+} Mice

In vivo experiments were performed 8 weeks after infection using an established protocol to elicit arrhythmias in RyR₂^{R4496C/+} mice through the intraperitoneal delivery of epinephrine and caffeine (2 and 120 mg/kg, respectively)^{4,10} and to compare arrhythmic events occurring in Het versus Het-U10 and Het-SCR mice (Figure 5A). Data showed that 52% of Het mice (11/21) and 65% of Het-SCR (15/23) mice exhibited the typical bidirectional ventricular tachycardia,⁸ although treatment with miR_{YR2}-U10 completely prevented the development of arrhythmias (0/25; Het-U10 versus Het-SCR, ****P*<0.001; Het-U10 versus Het, ****P*<0.001; Figure 5B).

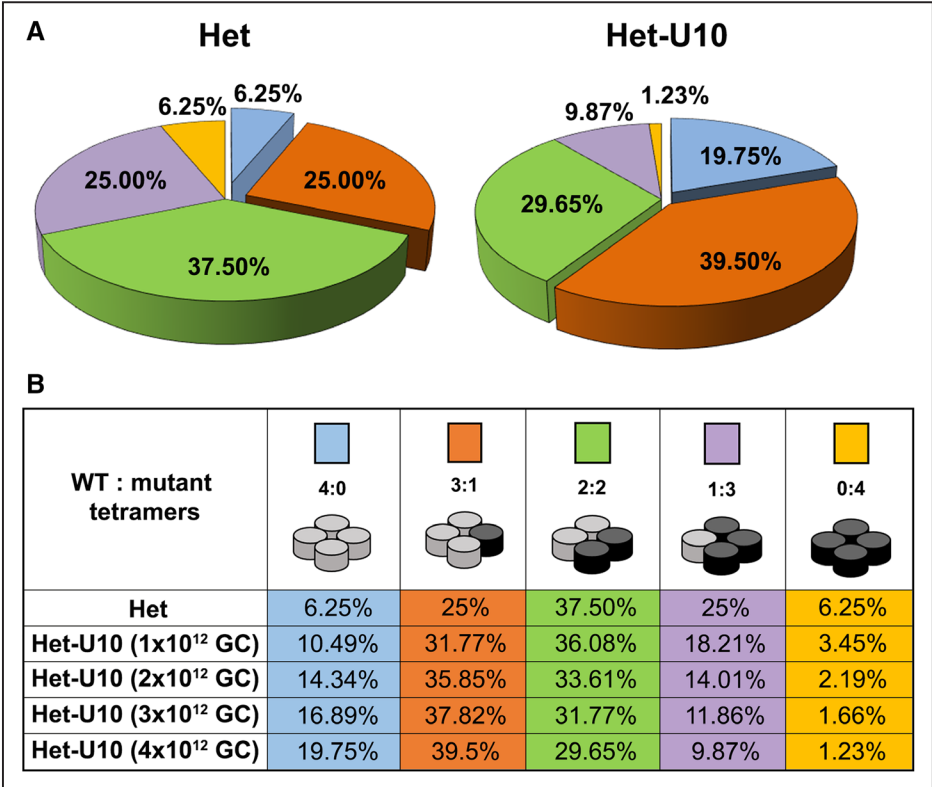


Figure 3. Likelihood for functional RyR2 (Ryanodine Receptor type 2 protein) tetramer formation with exposure to miR_{YR2}-U10. **A**, Modeling of the combination of mutant and wild-type (WT) RyR2 monomers to form the tetrameric channel assuming random assembly and applying a binomial distribution in the untreated heterozygous (Het [heterozygous RyR₂^{R4496C/+}]) and in the heterozygous mice treated at the dose of 3.9×10^{12} Genome Copies (GC; Het-U10 [heterozygous RyR₂^{R4496C/+} infected with AAV9-miR_{YR2}-U10]). **B**, Impact of increasing doses of AAV9-miR_{YR2}-U10 on the combination of WT (light grey); mutant (dark grey) monomers. AAV9 indicates adeno-associated serotype 9 viral vector. RyR₂^{R4496C/+} indicates mice heterozygous for the R4496C mutation in the Ryanodine Receptor 2 gene.

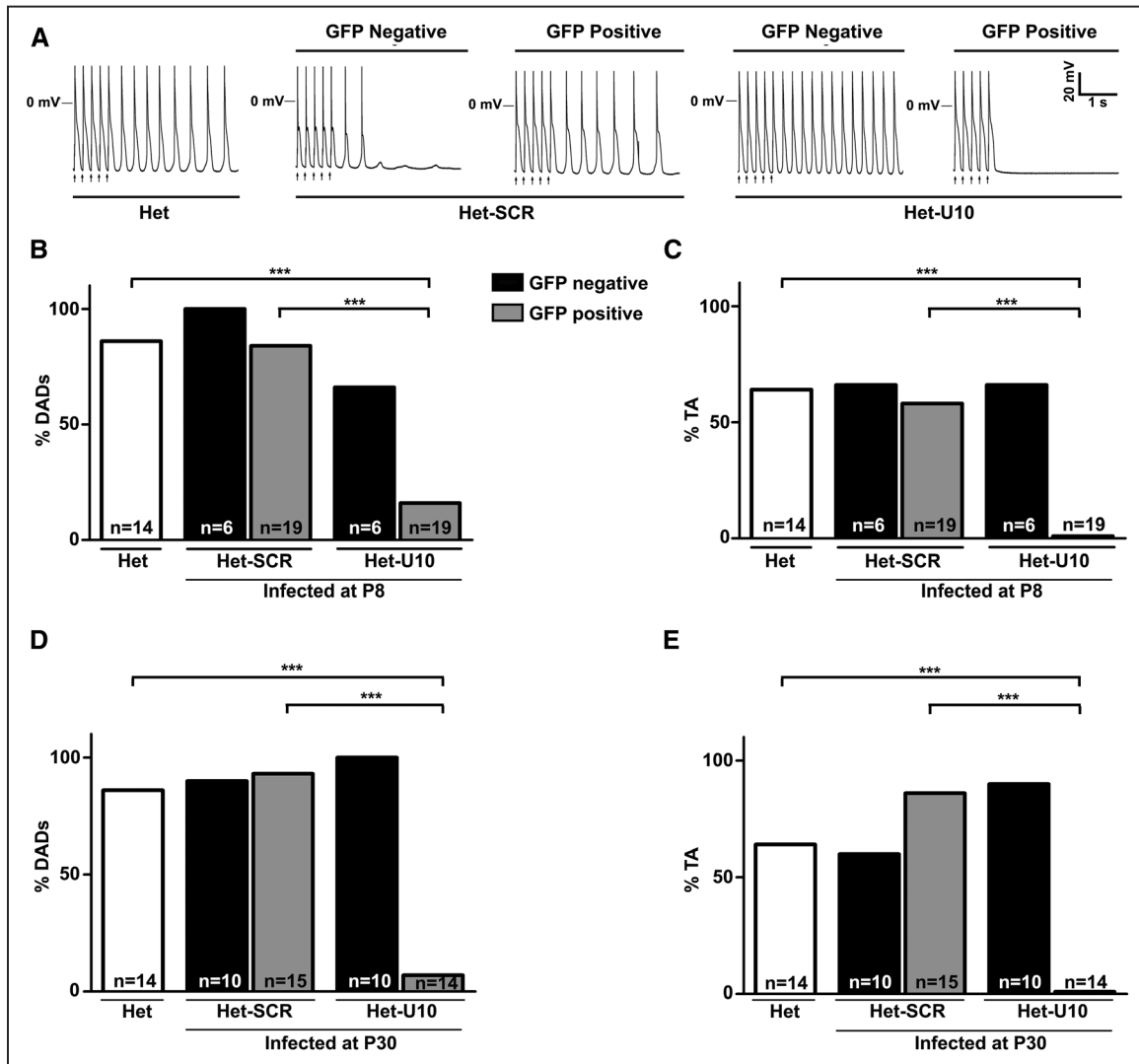


Figure 4. Electrophysiological evaluation of allele-specific silencing in $RyR2^{R4496C/+}$ mice. **A**, Action potentials elicited at 5 Hz (indicated by arrows) after exposure to 30 nmol/L isoproterenol (ISO) in isolated myocytes from $RyR2^{R4496C/+}$ untreated mice (Het [heterozygous $RyR2^{R4496C/+}$]) and in Het-SCR (heterozygous $RyR2^{R4496C/+}$ infected with AAV9-miRNA-Scramble) or Het-U10 (heterozygous $RyR2^{R4496C/+}$ infected with AAV9-miR2-U10). **B** and **C**, Quantification of the incidence of delayed afterdepolarizations (DADs) and triggered activity (TA) in cells derived from Het, Het-SCR, and Het-U10 infected at 8 d of age (p8; *** P <0.001). **D** and **E**, Quantification of the incidence of DADs and TA in cells derived from Het, Het-SCR, and Het-U10 infected at 30 d of age (p30; *** P <0.001). Number of animals per each group is indicated in the respective bar. Experiments were performed 8 wk after infection.

Similar results were observed in mice infected at 30 days after birth and studied 8 weeks after infection: a remarkable reduction of the ventricular tachycardia occurred in Het-U10 (2/24, 8%) in comparison with the Het-SCR (13/21, 62%) and Het mice (10/20, 50%; Het-U10 versus Het-SCR, *** P <0.001; Het-U10 versus Het, * P <0.016 [P =0.0051]; Figure 5C).

We performed a dose-response curve to determine the threshold for antiarrhythmic efficacy of AAV9-miR2-U10 in mice infected at 30 days after birth: as shown in Figure 5D, the antiarrhythmic efficacy appears at 3×10^{12} GC and it moderately further small improve at the dose we used in the in vivo study: 3.9×10^{12} GC.

Echocardiography showed no significant differences in ejection fraction and left ventricular diastolic diameter among heterozygous mice and mice treated with AAV9-miR2-U10 and AAV9-miRNA-Scramble. Data are presented in the Online Table I and Online Movie I.

Comparative Electron Microscopy Analysis of Heart Samples From WT, $RyR2^{R4496C/+}$, and $RyR2^{R4496C/+}$ Mice Treated With Allele-Specific Silencing

We performed electron microscopy on cardiac tissue of WT and Het mice to investigate whether, in analogy with mice with recessive CPVT,¹⁵ mice with the dominant form of CPVT present ultrastructural abnormalities. We observed structural alterations of the CRUs that, as shown in Figure 6, represent the contact area between the membranes of the jSR and the TT. On the surface of the jSR, the Ryanodine Receptor channels can be visualized (Figure 6A, small arrows). In WT cardiac myocytes, the jSR cisternae are usually narrow and flat. CASQ2 is clearly visible as a chain-like electron-dense line that runs parallel to the SR membrane (Figure 6A, single black arrow). In Het cardiac myocytes, the shape of jSR is more variable and slightly wider and does not always contain

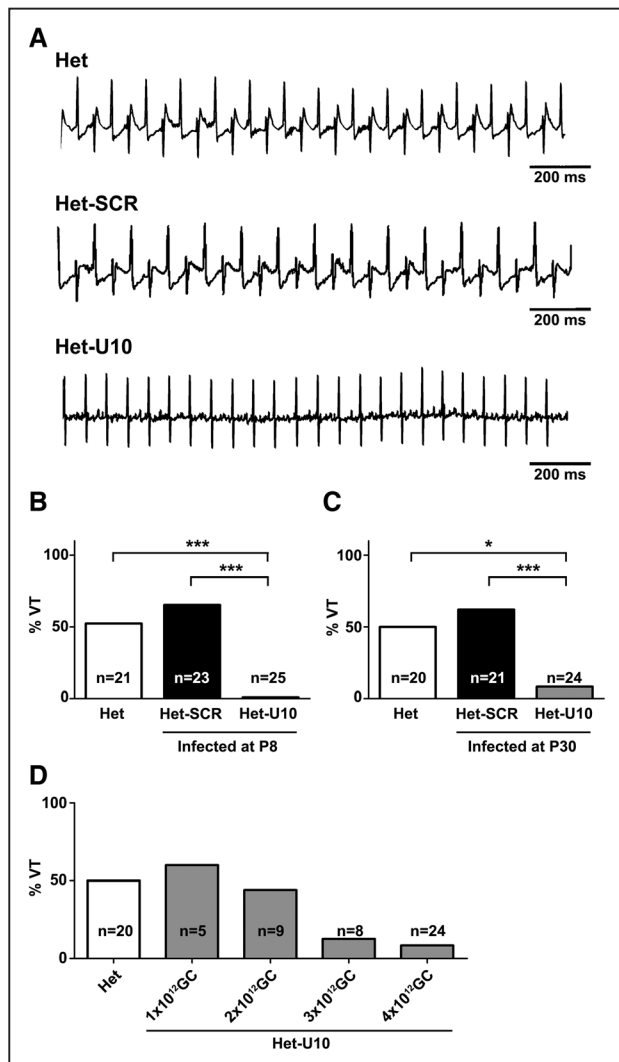


Figure 5. Evaluation of the incidence of ventricular arrhythmias after allele-specific silencing administration. **A**, In vivo epinephrine and caffeine administration elicited bidirectional ventricular tachycardia in Het (heterozygous *RyR2*^{R4496C/+}) and in Het-SCR (heterozygous *RyR2*^{R4496C/+} infected with AAV9-miRNA-Scramble), but not in Het-U10 (heterozygous *RyR2*^{R4496C/+} infected with AAV9-miR2-U10) mice. **B**, Incidence of ventricular tachycardia (VT) in Het, Het-SCR, and Het-U10 mice infected at 8 d (p8; ****P*<0.001). **C**, Quantification of the incidence of VT in Het, Het-SCR, and Het-U10 mice infected at 30 d (p30; **P*<0.016 (*P*=0.0051); ****P*<0.001). **D**, Quantification of incidence of VT in Het-U10 mice injected at p30 with increasing doses of AAV9-miR2-U10 Genome Copies (GC; approximate to single units): 1×10¹² GC, 2×10¹² GC, 3×10¹² GC, and 4×10¹² GC compared with untreated Het mice. The number of animals in each group is indicated in the bars. Experiments were performed 8 wk after infection.

the chain-like electron-dense polymer of *CASQ2* (Figure 6B); we think that the apparent reduction of *CASQ2* is most likely related to the increased volume of the abnormally enlarged jSR. In Het-SCR, cardiac myocytes CRUs appear as in Het cardiac myocytes (Figure 6C), although viral infection in Het-U10 rescues and restores the CRUs profile (Figure 6D).

When we compared the number of CRUs, the number of couplons, their length, and the jSR width, we observed that the number of CRUs, the number of couplons, and the

average length of individual couplon are reduced in Het mice when compared with WT (Online Table II). These abnormalities were superimposable to those previously reported in the *CASQ2*-R33Q mice,^{7,15} suggesting that these ultrastructural abnormalities are a common feature of CPVT models.¹⁶

When we analyzed Het-U10, we observed that most ultrastructural parameters were restored to normal values after the infection, whereas Het-SCR presented similar abnormalities as the nontreated mice (Het; Online Tables II and III).

Interestingly, we observed that although cardiac samples from WT mice have contractile elements well aligned laterally with each other and mitochondria distributed longitudinally between myofibrils that exhibit an electron-dense matrix with parallel and tightly packed internal cristae (Figure 7A), ~46% of myocytes from heart of Het mice presented damaged mitochondria with increased empty cytoplasmic spaces and alterations of the contractile elements (WT versus Het, **P*<0.001; Figure 7B and 7C; Online Figure VI). Of relevance, hearts treated with miR2-U10 (Het-U10; Figure 7E), but not those treated with miRNA-Scramble (Het-SCR; Figure 7D; Het-U10 versus Het-SCR, ‡*P*<0.005), showed a reduction in the percentage of cardiac cells with severe mitochondrial abnormalities (from 46% in Het to 28% in Het-U10; Het-U10 versus Het, †*P*<0.05; Figure 7F).

Discussion

The advancement of techniques to induce in vivo overexpression or silencing of selected genes has opened doors to the development of gene therapies to rescue the WT phenotype in carriers of inherited diseases. The applicability of gene therapy to inherited cardiac arrhythmias has not been explored mainly because of the concern that gene delivery could disrupt the highly regulated pattern of expression of proteins that regulate electric properties of the heart, thus aggravating, rather than improving, the arrhythmogenic substrate.¹⁷

We recently broke this conceptual barrier demonstrating that overexpression of cardiac *CASQ2* is beneficial in 2 animal models of recessive CPVT that manifests high propensity to arrhythmias caused by reduced levels of *CASQ2*. Our data showed that systemic intravenous delivery of the AAV9 construct containing WT *CASQ2* cDNA dramatically reduced arrhythmias in CPVT mice.^{7,18}

Here, we undertook a bigger challenge and attempted to rescue the WT phenotype in knock-in mice carriers of the pathogenic gain-of-function mutation R4496C in the *RyR2* gene associated with the CPVT phenotype. As we previously demonstrated, when exposed to β adrenergic activation, the frequency of calcium sparks in *RyR2*^{R4496C/+} mice is much higher than in WT animals.⁹ The same animal model is also prone to develop DADs and triggered arrhythmias that cannot be elicited in WT mice.⁴ We therefore speculated that the reduction of the amount of mutant protein induced by RNA interference targeted to the mutant allele could attenuate the development of arrhythmias.

We anticipated that even a partial reduction of mutant *RyR2* protein would be sufficient to attenuate arrhythmogenesis. The rationale behind our expectation was based on data from Xie et al¹⁹ who demonstrated that TA develops only when a sufficient number of adjacent cells develop DADs.

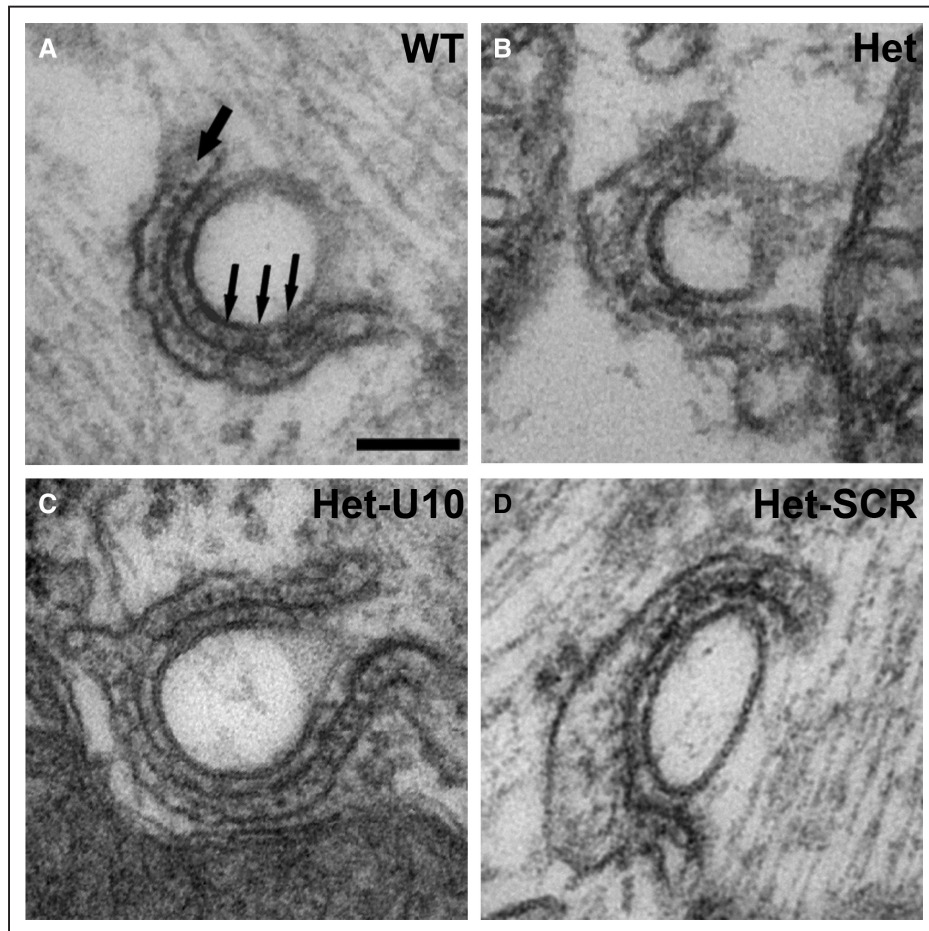


Figure 6. Electron microscopy analysis of calcium release units (CRUs) in wild-type (WT) and $RyR2^{R4496C/+}$ mice treated with allele-specific silencing. **A**, In WT cardiac myocytes, the junctional sarcoplasmic reticulum (jSR) cisternae are usually narrow and flat. Calsequestrin-2 (CASQ2) is clearly visible as a chain-like electron-dense line that runs parallel to the SR membrane (single black arrow). Smaller arrows in **A** point to the cytoplasmic domain, or feet, of RyR2s (Ryanodine Receptor type 2), spanning the narrow junctional gap between SR and plasmalemma. **B**, Het (heterozygous $RyR2^{R4496C/+}$) cardiac myocytes present an irregularly shaped and enlarged jSR that lacks the chain-like electron-dense polymer of CASQ2. **C**, Viral infection in Het-U10 rescues and restores the CRUs profile. **D**, In Het-SCR (heterozygous $RyR2^{R4496C/+}$ infected with AAV9-miRNA-Scramble) cardiac myocytes, CRUs seem as in Het cardiac myocytes. Measurements are reported in the Online Table II. Scale bar=0.1 μ m.

When this synchronization does not occur, afterdepolarizations are suppressed. In light of these data, we anticipated that even a partial reduction of mutant RyR2 would be able to exert an antiarrhythmic effect while limiting the risk of inducing an adverse reaction because of the loss of total RyR2 levels. This hypothesis is aligned with the results that we obtained when overexpressing the WT *CASQ2*⁷ in our homozygous recessive CPVT mouse model in which the infection of 40% of cardiac myocytes was sufficient to completely prevent arrhythmias.

The key challenge for our experimental plan is represented by the need to identify a siRNA able to selectively silence the mutant cDNA fragment containing the R4496C mutation while preserving unaltered the expression of the WT cDNA. Out of 13 screened siRNA, the best performing one (named siR2-U10) was able to silence the mutant transcript while leaving almost unaffected the expression of WT *RYR2* in HEK-293 cells. Analogously, its homologous artificial miRNA (miR2-U10) induced reduction of the expression of R4496C allele both at the mRNA and at the protein level without affecting WT expression in the same in vitro system.

The second challenge that we faced is represented by the unpredictable efficacy of the selected miRNA in vivo. We therefore treated the $RyR2^{R4496C/+}$ mice with AAV9-miR2-U10 and 8 weeks later assessed whether this treatment would protect the animals from the arrhythmogenic effect of the injection of caffeine and epinephrine. We observed a dramatic reduction of the inducibility of bidirectional and polymorphic ventricular tachycardia in both group of animals, that is, mice infected in the perinatal period (at day 8) and those infected at reproductive age (p30) when compared with untreated heterozygous mice and mice treated with AAV9-miRNA-Scramble. Aligned with the suppression of arrhythmias, experiments performed in isolated cells demonstrated that myocytes derived from the heart of mice infected with AAV9-miR2-U10, but not those infected with AAV9-miRNA-Scramble, showed abolition of DADs in fluorescent infected cells, whereas nonfluorescent cells responded to isoproterenol administration developing DADs and TA. These data support the concept that silencing of the mutant allele results in a powerful antiarrhythmic effect irrespective of the age of treatment.

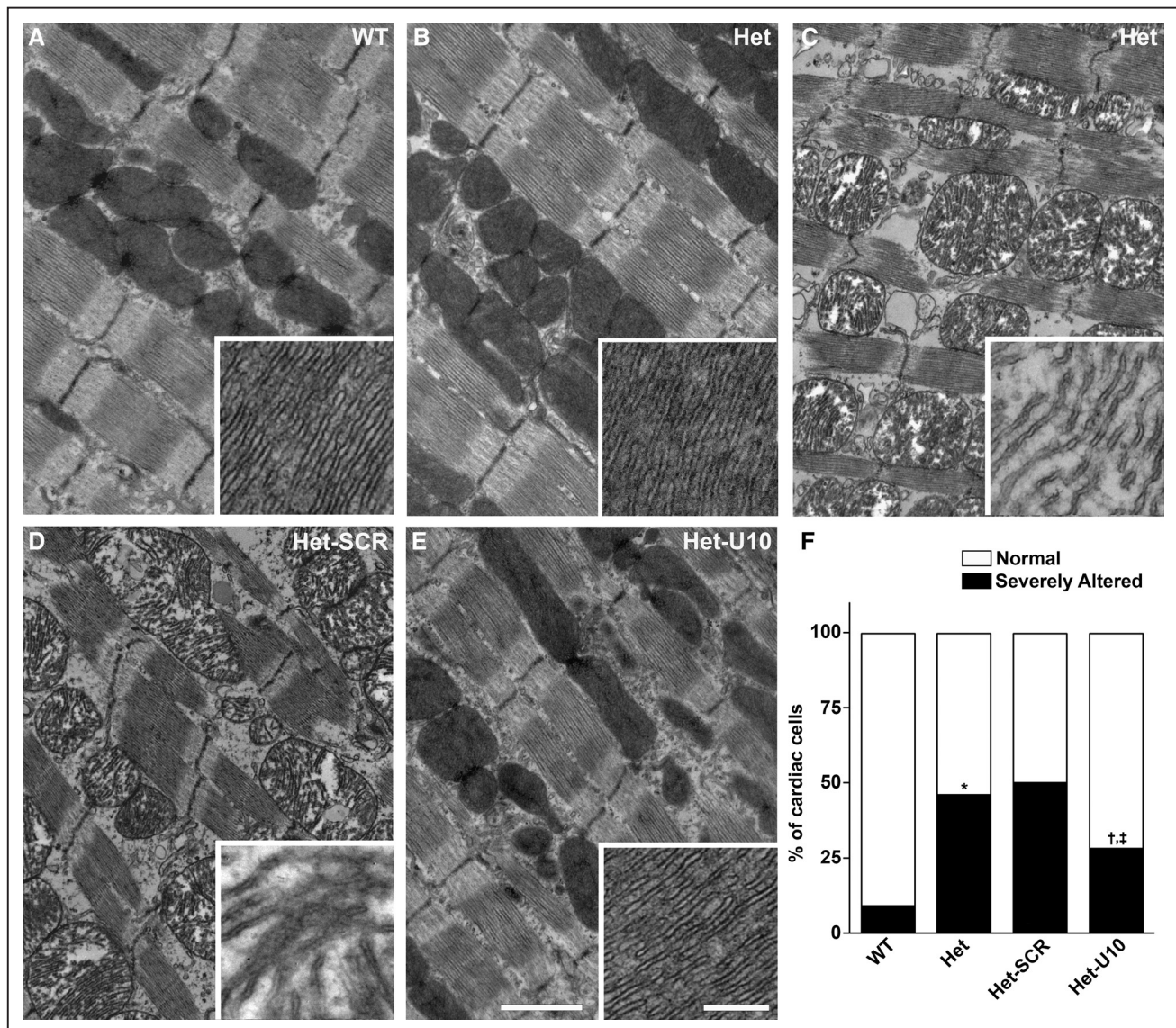


Figure 7. Electron microscopy analysis of contractile elements and mitochondria in wild-type (WT) and $RyR2^{R4496C/+}$ mice treated with allele-specific silencing. A–E, Representative electron micrographs of cardiac cells in WT (A), Het (heterozygous $RyR2^{R4496C/+}$; B and C), Het-SCR (heterozygous $RyR2^{R4496C/+}$ infected with AAV9-miRNA-Scramble; D), Het-U10 (heterozygous $RyR2^{R4496C/+}$ infected with AAV9-miR $RyR2$ -U10; E). Insets show a detail of mitochondrial internal cristae. F, Quantitative analysis of the percentage of cardiac cells presenting severe structural abnormalities (Het vs WT, $*P<0.001$; Het-U10 vs Het, $^{\dagger}P<0.05$; Het-U10 vs Het-SCR, $^{\ddagger}P<0.005$; $n=90$ cells from $n=3$ hearts each group). Scale bars=A–E, 1 μ m; insets, 0.2 μ m.

Applying the results of allele-specific real-time PCR, we simulated a binomial distribution of the WT and mutant $RyR2$ monomers in the formation of the tetrameric $RyR2$ structure and we derived that myocytes infected with the AAV9-mi $RyR2$ -U10, thanks to the selective inhibition of the transcription of the mutant allele, present an increase from 6.25% to 19.75% in the homomeric WT $RyR2$ channels (ie, $RyR2$ channels composed of 4 WT subunits) and a reduction from 6.25% to 1.23% of the homomeric mutant $RyR2$. Interestingly, when we performed a dose–response curve of the AAV9-mi $RyR2$ -U10, we observed that the antiarrhythmic efficacy parallels the predicted reduction of mutant versus WT $RyR2$ subunits (Figures 2E and 5D). The evidence that partial selective reduction of $RyR2$ mutant transcript attenuates arrhythmias in mice raises the novel concept that the

variability in the severity of clinical manifestations observed among CPVT patients within the same family may be related to the ratio between WT and mutant $RyR2$. Whether the relative amount of the WT $RyR2$ and the mutant $RyR2$ may also be modulated by posttranscriptional modifications and influenced by environmental factors is an intriguing hypothesis that may justify the paroxysmal nature of clinical manifestations in CPVT patients. Our interpretation of results is supported by data from Li and Chen²⁰ who showed that coexpression of the loss-of-function mutant E3987A and WT $RyR2$ protein in HEK-293 cells produces channels in which the reduction of the open probability of the channel is proportional to the number of the mutant monomers. It is therefore likely to assume that, in line with our observation, tetramers composed of a gain-of-function mutant and WT $RyR2$ protein would show

a larger increase in the open probability as the number of mutant subunits in the tetrameric channel augments.

An open question that we anticipated in designing our experimental protocol was represented by the unpredictable consequences of reducing the amount of total RyR2 on cardiac contractility. It is therefore reassuring to see that assessment of cardiac function by echocardiography, performed before testing inducibility of arrhythmias in mice, did not send signals of changes in the end-diastolic diameters of the heart and of reduction of the ejection fraction.

On the basis of the findings obtained in our recessive CPVT model in which AAV9-mediated expression of WT *CASQ2* not only rescued in vitro and in vivo phenotype but it was also able to recover the ultrastructural abnormalities of the jSR and the TT, we investigated whether targeted silencing of mutant RyR2 would normalize ultrastructural changes observed in Het mice and as expected both dilatation of jSR and fragmentation of TT were rescued by the treatment.

In this study, we also reported for the first time the presence of mitochondrial alterations in the heart of CPVT mice: this observation is relevant when placed in the context of the emerging evidence that mitochondrial alterations may occur in association with the presence of dysfunctional RyR channels in different tissues. The initial observation was made by 2 coauthors of this study (S.B. and F.P.) who reported back in 2009 the observation that a gain-of-function mutation in RyR1 (Y522S), causative for malignant hyperthermia, was associated with the development at young age of mitochondrial swelling and disruption that progressed with aging to cause local disruption of nearby SR and TT resulting in extreme sarcomere shortening and lack of mitochondria. The authors proposed that the Y522S mutation enhances SR Ca^{2+} leak, which, in turn, increases reactive oxygen species/reactive nitrogen species production and subsequent RYR1 S-nitrosylation and glutathionylation, further enhancing SR Ca^{2+} leak and release channel heat sensitivity. Both Ca^{2+} overload and increased redox stress promote activation of the mitochondrial permeability transition pore, the opening of which leads to mitochondrial depolarization, Ca^{2+} overload, and swelling.²¹ This hypothesis has not been tested, nor the presence of mitochondrial degeneration has been confirmed in humans; however, the observation has opened the field to further dwelling into the relationship between RyR2 dysfunction and mitochondrial disease.

Recently, Santulli et al²² showed that in the presence of a RyR2 mutation, functional and structural mitochondrial abnormalities develop in pancreatic β cells that express RyR2. The authors attribute the development of mitochondrial damage to the activation of the stress response in the endoplasmic reticulum in response to abnormal calcium leakage from the endoplasmic reticulum.

Finally, few months ago, Lavorato et al²³ published an intriguing study that shows that the A4860G *RYR2* loss-of-function mutation causes ultrastructural abnormalities in the heart of the mice characterized by the formation of nanotunnels in cardiac mitochondria. The authors suggested that the reduced release of calcium from the SR as a consequence of the primary mutation leads to random bursts of Ca^{2+} release because of Ca^{2+} overload in the SR leading to the formation of

nanotubules: in the study, the mechanisms linking Ca^{2+} overload and development of nanotubules remain unknown.

In this context, our observation that approximately half of myocytes from heart of Het mice present altered mitochondria with degeneration of crista and increased empty cytoplasmic spaces demonstrates for the first time that gain-of-function RyR2 mutations are associated with mitochondrial damage in the heart. The evidence that reducing the mutant *RYR2* transcripts through the delivery of our RNA-interference-based gene therapy rescues ultrastructural phenotype, supports the view of the existence of a causative link between RyR2 dysfunction and mitochondrial abnormalities. Although, the mechanisms linking RyR2 gating anomalies and degeneration of mitochondria in the heart remain to date undefined. Whether similar structural changes are present also in the heart of CPVT patients remains to be defined.

The ability of RNA interference to rescue the murine CPVT phenotype by preventing the development of TA in isolated cells, inhibiting the development of ventricular tachycardia in vivo and reverting ultrastructural abnormalities without causing adverse consequences, provides the proof of concept that mutant allele-specific silencing may evolve into a therapeutic strategy for CPVT patients.

Acknowledgments

We thank Patrizia Vaghi (Centro Grandi Strumenti of the University of Pavia) for technical assistance on Confocal Microscopy. We thank Vittorio Bellotti and Sofia Giorgetti for helpful suggestions and for the revision of the article.

Sources of Funding

We acknowledge the support of the following grants to S.G. Priori: European Research Council (ERC) 2015 to 2020 EU-rhythm no. 669387, the Intramural Research Grant 2015 to 2017 from the Fondazione Salvatore Maugeri.

Disclosures

S.G. Priori, C. Napolitano, and M. Denegri own shares of Audentes Therapeutics. The other authors report no conflicts.

References

1. Leenhardt A, Lucet V, Denjoy I, Grau F, Ngoc DD, Coumel P. Catecholaminergic polymorphic ventricular tachycardia in children. A 7-year follow-up of 21 patients. *Circulation*. 1995;91:1512–1519.
2. Priori SG, Napolitano C, Tiso N, Memmi M, Vignati G, Bloise R, Sorrentino V, Danieli GA. Mutations in the cardiac ryanodine receptor gene (hRyR2) underlie catecholaminergic polymorphic ventricular tachycardia. *Circulation*. 2001;103:196–200.
3. Bers DM. Cardiac excitation-contraction coupling. *Nature*. 2002;415:198–205. doi: 10.1038/415198a.
4. Liu N, Colombi B, Memmi M, Zissimopoulos S, Rizzi N, Negri S, Imbriani M, Napolitano C, Lai FA, Priori SG. Arrhythmogenesis in catecholaminergic polymorphic ventricular tachycardia: insights from a RyR2 R4496C knock-in mouse model. *Circ Res*. 2006;99:292–298. doi: 10.1161/01.RES.0000235869.50747.e1.
5. Hayashi M, Denjoy I, Hayashi M, Extramiana F, Maltret A, Roux-Buisson N, Lupoglazoff JM, Klug D, Maury P, Messali A, Guicheney P, Leenhardt A. The role of stress test for predicting genetic mutations and future cardiac events in asymptomatic relatives of catecholaminergic polymorphic ventricular tachycardia probands. *Europace*. 2012;14:1344–1351. doi: 10.1093/europace/eus031.
6. Priori SG, Blomström-Lundqvist C, Mazzanti A. 2015 ESC Guidelines for the management of patients with ventricular arrhythmias and the prevention of sudden cardiac death. *Eur Heart J*. 2015;36:2793–2861.

7. Denegri M, Bongianino R, Lodola F, et al. Single delivery of an adeno-associated viral construct to transfer the CASQ2 gene to knock-in mice affected by catecholaminergic polymorphic ventricular tachycardia is able to cure the disease from birth to advanced age. *Circulation*. 2014;129:2673–2681. doi: 10.1161/CIRCULATIONAHA.113.006901.
8. Cerrone M, Colombi B, Santoro M, di Barletta MR, Scelsi M, Villani L, Napolitano C, Priori SG. Bidirectional ventricular tachycardia and fibrillation elicited in a knock-in mouse model carrier of a mutation in the cardiac ryanodine receptor. *Circ Res*. 2005;96:e77–e82. doi: 10.1161/01.RES.0000169067.51055.72.
9. Cerrone M, Noujaim SF, Tolkacheva EG, Talkachou A, O'Connell R, Berenfeld O, Anumonwo J, Pandit SV, Vikstrom K, Napolitano C, Priori SG, Jalife J. Arrhythmogenic mechanisms in a mouse model of catecholaminergic polymorphic ventricular tachycardia. *Circ Res*. 2007;101:1039–1048. doi: 10.1161/CIRCRESAHA.107.148064.
10. Liu N, Ruan Y, Denegri M, Bachetti T, Li Y, Colombi B, Napolitano C, Coetzee WA, Priori SG. Calmodulin kinase II inhibition prevents arrhythmias in RyR2(R4496C+/-) mice with catecholaminergic polymorphic ventricular tachycardia. *J Mol Cell Cardiol*. 2011;50:214–222. doi: 10.1016/j.yjmcc.2010.10.001.
11. Pacak CA, Mah CS, Thattaliyath BD, Conlon TJ, Lewis MA, Cloutier DE, Zolotukhin I, Tarantal AF, Byrne BJ. Recombinant adeno-associated virus serotype 9 leads to preferential cardiac transduction in vivo. *Circ Res*. 2006;99:e3–e9. doi: 10.1161/01.RES.0000237661.18885.f6.
12. Loud AV, Barany WC, Pack BA. Quantitative evaluation of cytoplasmic structures in electron micrographs. *Lab Invest*. 1965;14:996–1008.
13. Mobley BA, Eisenberg BR. Sizes of components in frog skeletal muscle measured by methods of stereology. *J Gen Physiol*. 1975;66:31–45.
14. Chan WM, Siu WY, Lau A, Poon RY. How many mutant p53 molecules are needed to inactivate a tetramer? *Mol Cell Biol*. 2004;24:3536–3551.
15. Rizzi N, Liu N, Napolitano C, et al. Unexpected structural and functional consequences of the R33Q homozygous mutation in cardiac calsequestrin: a complex arrhythmogenic cascade in a knock in mouse model. *Circ Res*. 2008;103:298–306. doi: 10.1161/CIRCRESAHA.108.171660.
16. Chopra N, Knollmann BC. Cardiac calsequestrin: the new kid on the block in arrhythmias. *J Cardiovasc Electrophysiol*. 2009;20:1179–1185. doi: 10.1111/j.1540-8167.2009.01531.x.
17. Bongianino R, Priori SG. Gene therapy to treat cardiac arrhythmias. *Nat Rev Cardiol*. 2015;12:531–546. doi: 10.1038/nrcardio.2015.61.
18. Denegri M, Avelino-Cruz JE, Boncompagni S, De Simone SA, Auricchio A, Villani L, Volpe P, Protasi F, Napolitano C, Priori SG. Viral gene transfer rescues arrhythmogenic phenotype and ultrastructural abnormalities in adult calsequestrin-null mice with inherited arrhythmias. *Circ Res*. 2012;110:663–668. doi: 10.1161/CIRCRESAHA.111.263939.
19. Xie Y, Sato D, Garfinkel A, Qu Z, Weiss JN. So little source, so much sink: requirements for afterdepolarizations to propagate in tissue. *Biophys J*. 2010;99:1408–1415. doi: 10.1016/j.bpj.2010.06.042.
20. Li P, Chen SR. Molecular basis of Ca(2)+ activation of the mouse cardiac Ca(2)+ release channel (ryanodine receptor). *J Gen Physiol*. 2001;118:33–44.
21. Boncompagni S, Rossi AE, Micaroni M, Hamilton SL, Dirksen RT, Franzini-Armstrong C, Protasi F. Characterization and temporal development of cores in a mouse model of malignant hyperthermia. *Proc Natl Acad Sci USA*. 2009;106:21996–22001. doi: 10.1073/pnas.0911496106.
22. Santulli G, Pagano G, Sardu C, Xie W, Reiken S, D'Ascia SL, Cannone M, Marziliano N, Trimarco B, Guise TA, Lacampagne A, Marks AR. Calcium release channel RyR2 regulates insulin release and glucose homeostasis. *J Clin Invest*. 2015;125:1968–1978. doi: 10.1172/JCI79273.
23. Lavorato M, Iyer VR, Dewight W, Cupo RR, Debattisti V, Gomez L, De la Fuente S, Zhao YT, Valdivia HH, Hajnóczky G, Franzini-Armstrong C. Increased mitochondrial nanotunneling activity, induced by calcium imbalance, affects intermitochondrial matrix exchanges. *Proc Natl Acad Sci USA*. 2017;114:E849–E858. doi: 10.1073/pnas.1617788113.

Allele-Specific Silencing of Mutant mRNA Rescues Ultrastructural and Arrhythmic Phenotype in Mice Carriers of the R4496C Mutation in the Ryanodine Receptor Gene (*RYR2*)

Rossana Bongianino, Marco Denegri, Andrea Mazzanti, Francesco Lodola, Alessandra Vollero, Simona Boncompagni, Silvia Fasciano, Giulia Rizzo, Damiano Mangione, Serena Barbaro, Alessia Di Fonso, Carlo Napolitano, Alberto Auricchio, Feliciano Protasi and Silvia G. Priori

Circ Res. 2017;121:525-536; originally published online June 15, 2017;

doi: 10.1161/CIRCRESAHA.117.310882

Circulation Research is published by the American Heart Association, 7272 Greenville Avenue, Dallas, TX 75231

Copyright © 2017 American Heart Association, Inc. All rights reserved.

Print ISSN: 0009-7330. Online ISSN: 1524-4571

The online version of this article, along with updated information and services, is located on the World Wide Web at:

<http://circres.ahajournals.org/content/121/5/525>

Data Supplement (unedited) at:

<http://circres.ahajournals.org/content/suppl/2017/06/15/CIRCRESAHA.117.310882.DC1>

Permissions: Requests for permissions to reproduce figures, tables, or portions of articles originally published in *Circulation Research* can be obtained via RightsLink, a service of the Copyright Clearance Center, not the Editorial Office. Once the online version of the published article for which permission is being requested is located, click Request Permissions in the middle column of the Web page under Services. Further information about this process is available in the [Permissions and Rights Question and Answer](#) document.

Reprints: Information about reprints can be found online at:

<http://www.lww.com/reprints>

Subscriptions: Information about subscribing to *Circulation Research* is online at:

<http://circres.ahajournals.org/subscriptions/>

SUPPLEMENTAL MATERIAL

Detailed Methods

Cloning of reporter alleles and siRNA design

Sequence encompassing exon 91 to 96 of the murine *RYR2* gene was amplified from wild-type (WT) mouse cDNA using primers containing adapters for SacI and EcoRI restriction enzymes (RYR2_91-SacI-FOR:

5' _CTGAGCTCTCGAGCAGAAGGCGAAAGAGG_3'; RYR2_96-EcoRI-REV:

5' _CTGAATTCCTTTCTTTTCACAAATTTATCCC_3'), digested and ligated into pZFN1 (Sigma-Aldrich), upstream of the 3XFLAG tag sequence (MDYKDHDGDYKDHDIDYKDDDDK). Subsequently *RYR2_ex91-96_3xFLAG* was amplified using primers containing adapters for SacI and KpnI (RYR2_91-SacI-FOR: 5' _CTGAGCTCTCGAGCAGAAGGCGAAAGAGG_3'; 3XFLAG-KpnI-REV:

5' _CTGGTACCCTTGTCATCGTCATCCTTGTAAATCG_3') and sub-cloned into pEGFP-C1 plasmid (Clontech), downstream the Green Fluorescent Protein (GFP). The resulting plasmid was subjected to site directed mutagenesis to generate the R4496C mutation in the encoded protein, using the following primers: R4496C-RYR2-FOR: 5' _CTTCTAAACTATTTTGCTTGCAACTTTTACAACATGAG_3'; R4496C-RYR2-REV: 5' _CTCATGTTGTAAAAGTTGCAAGCAAAATAGTTTAGAAG_3', through Quickchange Site-directed mutagenesis kit (Stratagene) according to the manufacturer's indications.

In parallel exon 91 to 96 were amplified from wild-type mouse cDNA using another couple of primers containing adapters for SacI and XhoI restriction enzymes (RYR2_91-SacI-FOR:

5' _CTGAGCTCTCGAGCAGAAGGCGAAAGAGG_3'; RYR2_96-XhoI-REV:

5' _CCCTCGAGCTTTCTTTTCACAAATTTATCCC_3') digested and ligated into pIRES-hrGFP-2a (Agilent Technologies), upstream of the 3XHA tag sequence

(YPYDVPDYAYPYDVPDYAYPYDVPDYA). Subsequently *RYR2_ex91-96_3xHA* was amplified using primers containing adapters for SacI and KpnI enzymes (RYR2_ex91_SacI-FOR:

5' _CTGAGCTCTCGAGCAGAAGGCGAAAGAGG_3'; 3XHA-KpnI-REV:

5' _CTGGTAACCTATTAAGCGTAGTCAGGTAC_3') digested and sub-cloned into pEGFP-C1 (BD Biosciences Clontech) downstream the Green Fluorescent Protein (GFP). From the resulting plasmid GFP coding sequence was excised using NheI and BglII and replaced with RFP coding sequence that was obtained by PCR amplification with primers containing adapters for NheI and BglII restriction enzymes (RFP-NheI-FOR: 5' _CAGCTAGCATGGTGAGCAAGGGCG_3'; RFP-BglII-REV:

5' _GTAGATCTCTTGTACAGCTCGTCCATGCC_3') from pmCHERRY-N1 (Clontech) and properly digested. Each cloning step was carefully designed and controlled to maintain the reading frame (ORF) from the fluorescent protein gene through the *RYR2* cDNA until the tag sequence.

These two plasmids were used as reporter alleles containing the following functional cassettes:

1) pEGFP_RYR2ex91-96/R4496C_3xFLAG;

2) pRFP_RYR2ex91-96/WT_3xHA.

siRNAs against mutant *RYR2* were designed based on mutant recognition site shift from position 5 to position 17 to optimally study difference in discrimination parameters and ordered as RNA duplexes (Sigma-Aldrich) with dTdT 3' modification.

RNA extraction, retrotranscription and semi-quantitative Real-time PCR

HEK-293 transiently transfected with equal amount of the reporter alleles and RNAi molecules were lysed and total RNA was purified with RNeasy mini kit (Qiagen). RNeasy Fibrous Tissue mini kit (Qiagen) was used for RNA extraction from isolated hearts and other organs derived from infected mice. An on-column DNaseI (Qiagen) digestion was performed for each sample for 15 min at room temperature.

A total amount of 1 µg template RNA per reaction was used for a 20 µl retrotranscription, performed with iScript cDNA Synthesis kit (Bio-Rad) in according with the manufacturer's instruction.

Real-time PCR was performed using the CFX96 Real-Time PCR Detection System and analyzed using the Bio-Rad CFX Manager software package (Bio-Rad). Quantitative Real-time PCR analysis was performed in optical 96-well in triplicate with SsoFast EvaGreen Supermix (Bio-Rad) using specific primer mix to selectively amplify GFP or RFP sequence (GFP-FOR: 5' _CTATATCATGGCCGACAAGCAG_3', GFP-REV: 5' _GCTCGTCCATGCCGAGCGTG_3', RFP-FOR: 5' _GCGTGATGAACTTCGAGGACG_3', RFP-REV: 5' _CAGCCCATGGTCTTCTTCTGC_3'), FLAG or HA (RYR2-FOR:

5' _GAACCTCCAGCGATACTGC_3', FLAG-REV:

5' _CTGGTACCCTTGTCATCGTCATCCTTGTAAATCG_3', HA-REV

5'_CTGGTACCCTATTAAGCGTAGTCAGGTAC_3'), to quantify mutated allele or wild-type mRNA respectively, and 20 ng of cDNA template. GAPDH was used as internal reference using the following primers: GAPDH-FOR: 5'_AAATCCCATCACCATCTTCC_3' and GAPDH-REV: 5'_GGTTCACACCCATGACGAAC_3'.

Total RYR2 transcript levels were evaluated in cardiac tissue using the following primers: mRYR2-FOR: 5'_CCTTTATAACCGGACTCGACG_3' and mRYR2-REV: 5'_TTGGCCCATATGTTGTGGTAG_5'.

Murine GAPDH was used as internal reference using the following primers: mGAPDH-FOR: 5'_GAAAGCTGTGGCGGTGATG_3' and mGAPDH-REV: 5'_GCCCAAGATGCCCTTCAGTG_3'.

Protein extraction and immunoblotting

HEK-293 cells transiently transfected with equal amount of the reporter alleles and RNAi molecules were lysed in RIPA buffer (50 mM Tris HCl, pH 8.0, 150 mM NaCl, 1% NP-40, 0.5% sodium deoxycholate, 0.1% SDS and 1 mM EDTA) containing a cocktail of 1X protease inhibitors (Sigma-Aldrich). Total proteins (30 µg/sample), quantified by Pierce® BCA Protein Assay Kit (Thermo Scientific), were resolved by SDS-gel electrophoresis on Mini PROTEAN TGX Stain-Free 4-15% gradient Gels (Bio-Rad) using 1X Tris/Glycine/SDS buffer (Bio-Rad), and blotted on 0.2 µm nitrocellulose using Trans Blot Turbo Transfer System (Bio-Rad). The nitrocellulose membrane was saturated with a solution of TBS 1x, 0.1% Tween 20 (TBS-T, Sigma-Aldrich) and 5% Skin Milk. After blocking, the membrane was washed three times in TBS-T. The membranes were probed with different antibodies diluted in BSA 3% in TBS-T: anti-FLAG (F3165-Sigma-Aldrich), anti-HA (H3663-Sigma-Aldrich) and anti-pan cadherin (C1821-Sigma-Aldrich) as reference protein. Secondary antibodies, conjugated with HRP (Promega), were diluted in BSA 3% in TBS-T. Quantification of protein expression has been performed by densitometry of HA and FLAG bands normalized on the reference protein Pan Cadherin.

For protein extraction from cardiac tissue of treated and control mice, hearts were excised from euthanized mice, washed in ice cold PBS to remove excess of blood and immediately frozen in liquid nitrogen. Frozen heart were then homogenized using a mortar and a pestle in presence of liquid nitrogen. The pellet was washed in PBS and homogenized in 6 volumes of: 30 mM KH₂PO₄ (pH=7.0), 40 mM NaF, 5mM EDTA, 300 mM sucrose, 0.5 mM DTT containing a cocktail of 2X protease inhibitors (Sigma-Aldrich). Homogenates were then solubilized in 1 volume of 100 mM Tris-HCl (pH=7.4) and 6% SDS for 1 hour at room temperature. Insoluble particles were then removed by centrifugation at 21000 g for 10 minutes at 4°C. The proteins in the supernatant were quantified and 20 µg/sample were separated by SDS-PAGE on Mini PROTEAN TGX Stain-Free 4-15% gradient Gels (Bio-Rad) using 1X Tris/Glycine/SDS buffer (Bio-Rad) and blotted at 45 V for 15-20 hours at 4°C on 0.45 µm nitrocellulose using Mini Trans Blot System (Bio-Rad) in the presence of 0.01% SDS. Membranes were saturated with a solution of TBS 1X, 0.1% Tween 20 (TBS-T, Sigma-Aldrich) and 5% Skin Milk. Used primary antibodies diluted in 3% BSA in TBS-T were: anti-RyR2 (MA3-916 -Thermo Scientific) and anti-pan cadherin (C1821- Sigma-Aldrich) as reference protein. Secondary anti-Mouse antibody, conjugated with HRP (Promega), was diluted in 3% BSA in TBS-T. Immunoblotting membranes were revealed using the Clarity Western ECL substrate (Bio-Rad) and detected using ChemiDoc MP Imaging System (Bio-Rad). Quantification of protein expression has been performed by densitometry of RyR2 bands normalized on the reference protein Pan Cadherin.

Fluorescence microscopy

HEK-293 cells transiently transfected with reporter alleles and RNAi molecules were fixed on coverslips in 3.7% paraformaldehyde for 10 minutes at room temperature. Coverslips were then washed in phosphate-buffered saline (PBS) with gentle shaking and mounted with mounting medium (Dako Fluorescent Mounting Medium). Fluorescence images were obtained with a Leica TCS-SP2 digital scanning confocal microscope equipped with a HCX PL APO 40x/numerical aperture =1.25 oil immersion objective. We used 488-nm Argon laser line for excitation of GFP and He/Ne laser line at 580-630 nm for RFP. The pinhole diameter was kept at Airy 1. Images were exported to Adobe Photoshop (Adobe Systems, Mountain View, CA).

Artificial miRNA expressing vector design and production

The siRYR2-U10 siRNA duplex sequences, designed to target RYR2 mRNA containing the R4496C mutation, was cloned into a commercially available artificial miRNA expression vector (BLOCK-iT Pol II miR RNAi Expression vector, Life Technologies), that allows continuous and long-term expression of the silencing molecule. The cloning procedure was based on ligation of the following annealed oligonucleotides:

- 1) 5'_TGCTGTAAAAGTTGCAAGCAAAATAGTTTTG_3',
- 2) 5'_GCCACTGACTGACTATTTTGCGCAACTTTTAC_3',
- 3) 5'_CCTGGTAAAAGTTGCGCAAAATAGTCAGTCA_3',

4) 5'_GTGGCCAAACTATTTTGCTTGCAACTTTTAC_3'

with the linearized vector pcDNA_6.2-GW/EmGFPmiR (Life Technologies).

It was generated also the pcDNA_6.2-GW/EmGFP-miR-neg control plasmid containing an insert that can form a hairpin structure that is processed into mature miRNA, but is predicted not to target any known vertebrate gene. The negative control miRNA sequence is:

5'_GAAATGTACTGCGCGTGGAGACGTTTTGGCCACTGACTGACGTCTCCACGCAGTACATTT_3' (Life Technologies).

From the obtained plasmids, a fragment consisting in CMV promoter, EmGFP, pre-miRNA sequence and TKpolyA was amplified by PCR with specific primers (FOR:

5'_TAGCTAGCTGCTTCGCGATGTACGG_3' and REV

5'_GTGAATTCGAACAAACGACCCAACACCCG_3' including the NheI (FOR) and EcoRI (REV) cloning site and inserted into the Adeno-Associated viral backbone vector pAAV-2.1 provided by the Adeno-Associated Virus (AAV) vector core facility (Tigem, Napoli, Italy).

The AAV production was done in collaboration with the Tigem core facility (<http://www.tigem.it/core-facilities/adeno-associated-virus-aav-vector-core>).

Animal Model

In this study we used heterozygous RyR2^{R4496C/+} (Het) knock-in mice (patent US7741529 B1) previously characterized in our laboratory¹⁻³. Animals were raised and bred at Charles River (Calco, Italy). All mice were C57BL/6N and have been maintained and reproduced without interruption since 2005 at Charles River. Experiments were performed in animals of both genders and no differences were present across genders. Control animals were wild type littermates. Before any manipulation animals were anesthetized with Isoflurane (Isoflurane-Vet, Merial) using the apparatus (VisualSonics VevoTM Compact Anesthesia System). Animals were sacrificed by cervical dislocation.

Action potential recordings in isolated ventricular myocytes

Isolated ventricular myocytes were seeded on a glass bottom perfusion chamber mounted on the stage of an inverted microscope. After 5 minutes, the myocytes were bathed in the following solution at 35°C (in mmol/L): 140 NaCl, 4 KCl, 2 CaCl₂, 1 MgCl₂, 10 HEPES, and 5 Glucose, pH 7.4, with NaOH (Sigma-Aldrich). Action potential recording was performed using patch electrodes made of borosilicated (resistance of 2 to 3 MΩ) and filled with a solution containing: (in mmol/L): 120 potassium aspartate, 20 KCl, 1 MgCl₂, 4 Na₂ATP, 0.1 GTP, 10 HEPES, 10 Glucose, pH 7.2, with NaOH. Signals were acquired at 10 kHz (Digidata 1322A, Axon Instruments) and analyzed with pCLAMP version 9.2 software (Axon Instruments). Quiescent, calcium-tolerant, rod-shaped cells with clear cross striations and a resting potential < -80 mV were electrically stimulated using depolarizing pulses with duration of 3 ms and amplitude of 1.5 fold the minimal current needed to evoke an action potential. Correction for the liquid junction potential between pipette and bath solution was performed.

Allele-specific quantitative Real-time PCR

Samples obtained from treated and control mice were evaluated for *RYR2* allelic expression imbalance using quantitative Real-time PCR and allele-specific TaqMan probes that contain a minor groove binder (MGB) at the 3' end (p.Arg4496: VIC- TTTGTA AAAAGTTGCGAGCAAAA-MGB; p.Cys4496: FAM- TTTGTA AAAAGTTGCAAGCAAAA-MGB; allele-specific sequences are underlined) to quantify the separate alleles. Amplification primers (FOR: 5'_CTACCAACAGAAGCTGCTGAACTAT_3'; REV: 5'_CAAACAAGGCCAGCATTCTCATG_3') used in the assay generated a 68 bp amplicon with a two-temperature cycling protocol (95°C for 10 min followed by 45 cycles of 95°C, 15 s and 60°C, 1 min). Under these conditions, neither TaqMan probe exhibited cross-reactivity with the opposite allele. All reactions were performed on an Applied Biosystems ViiA7 Real-Time PCR System (Applied Biosystems). Individual reactions (20 µl) contained 2X TaqMan Genotyping Mix (Applied Biosystems), 40X Custom Taqman SNP Genotyping Assay mix containing both the specific primers and the probes, and 2 µl of cDNA. A standard curve was constructed by mixing the normal and mutant cDNA samples (created by retro-transcription of wild-type and homozygous RyR2^{R4496C/R4496C} heart tissue-derived RNA) to allelic ratios of 8, 4, 2, 1, 0.5, 0.25, and 0.125 in a total concentration of 10 ng/µl. The standard curve generated from assaying wild-type and homozygous cDNA mixed at known ratios and fitted with the equation $\log_2(\text{WT: R4496C ratio}) = \alpha \Delta C_T + \beta$ (α and β are fit parameters) was used to interpolate the ratio of allele expression for miR^{YR2-U10} infected and control samples.

Immunofluorescence on heart sections and image analysis

Hearts were collected, cannulated, washed with saline solution and fixed in 3.7% paraformaldehyde in PBS for 1 hour at 4°C. After washing three times in PBS for 5 min, hearts were equilibrated with 15% sucrose in PBS for 1 hour and incubated in 30% sucrose overnight at 4°C. Samples were included in OCT (Dako), and 4µm cryosections were prepared for immunofluorescence. Tissues were permeabilized with PBS-0.2% Triton (PBS-T) for 10 min, and washed in PBS. Tissues were blocked with 10% goat serum in PBS-T for 1 hour. Antibody against sarcomeric α -actinin (A7811 - Sigma-Aldrich) was diluted in PBS-10% goat serum (Sigma-Aldrich) and slides were incubated for 1 hour at room temperature. After washes, slides were incubated with anti-GFP 488-conjugated (600-141-215 Rockland) or Alexa Fluor 594-conjugated goat anti-mouse secondary antibodies (A11005 - Life Technologies) for 45 min followed by 1 minute in the presence of DAPI. Dako mounting medium was applied to all slides. Fluorescence images were obtained with a Leica TCS-SP2 inverted confocal microscope as described above.

Electron microscopy

Hearts isolated from WT, heterozygous RyR2^{R4496C/+} and infected heterozygous RyR2^{R4496C/+} mice, were fixed by retrograde aortic perfusion with 3.5% glutaraldehyde in 0.1 mol/L NaCaCo buffer (pH 7.2) and analyzed. Small bundles of papillary muscles were post-fixed in 2% OsO₄ in NaCaCo buffer for 2 hours and then block-stained in saturated uranyl acetate. After dehydration, specimens were embedded in an epoxy resin (Epon 812). Ultrathin sections were cut in a Leica Ultracut R microtome (Leica Microsystem, Austria) using a Diatome diamond knife (Diatome Ltd. CH-2501 Biel, Switzerland) and double stained with uranyl acetate and lead citrate. All sections were examined with an FP 505 Morgagni Series 268D electron microscope (FEI Company, Brno, Czech Republic), equipped with Megaview III digital camera and Soft Imaging System (Munster, Germany).

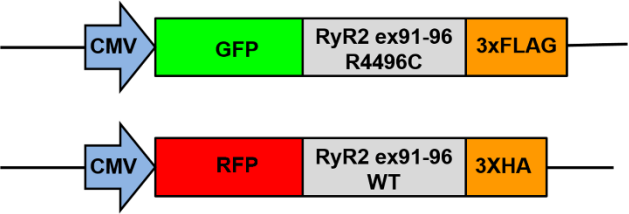
Quantitative analysis of electron microscopy images

The percentage of cardiac cells exhibiting severe structural alterations was quantified. Cells considered *severely damaged* are characterized by severe structural abnormalities affecting mitochondria in the majority of the interior. In most cases, cardiac cells with severely altered mitochondria also present large area of apparently empty cytoplasmic spaces and alterations affecting contractile elements. Sample size: 3 different hearts from each of the 4 group of samples (n=30 cells in each heart).

Cytoplasmic, mitochondrial, and SR volume were calculated by the well-established stereology point-counting technique^{4,5} in micrographs taken at 22.000 of magnification from cross-sections of papillary cardiomyocytes. For each sample, 3 hearts were analysed and more of 65 cells quantified. In each cardiac cell, 2 pictures were taken in internal areas, excluding the nuclei and Golgi regions. The images were covered with an orthogonal array of dots at a spacing of 0.35 µm and the ratio between numbers of dots falling within cytoplasmic space, mitochondria and SR membranes over the total number of dots covering the whole image was used to calculate the relative cell volume.

Supplemental Figures and Figure Legends

A



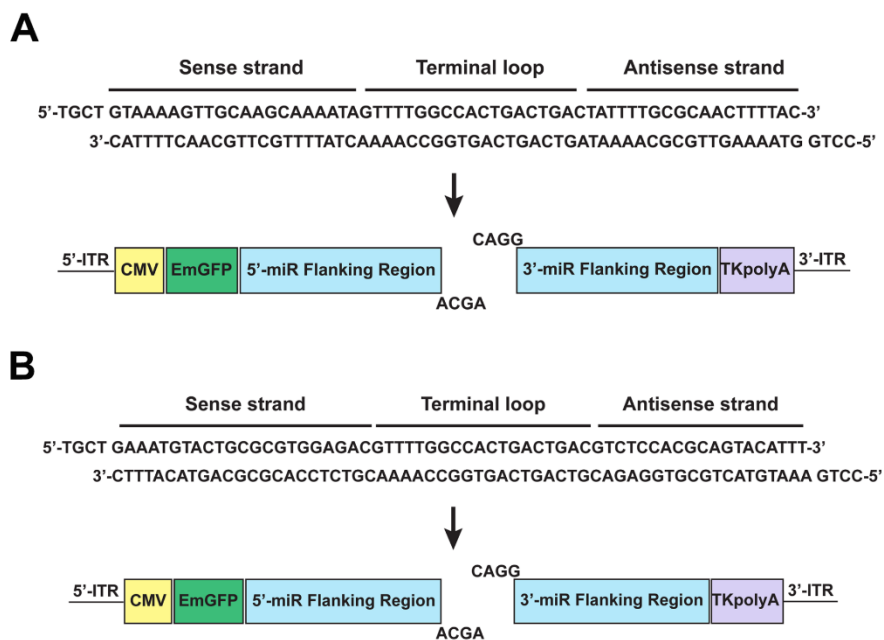
B

Wild Type RYR2 mRNA :
5'- AACAGAAGCUGCUGAACUAUUUUGCU^CGCAACUUUUACAACAUGAGAAUGCUGGCC-3'

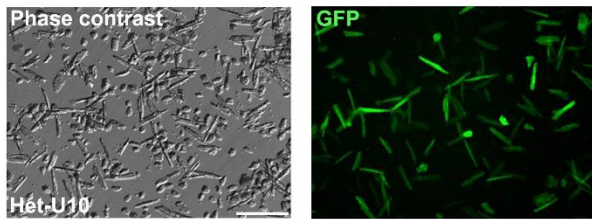
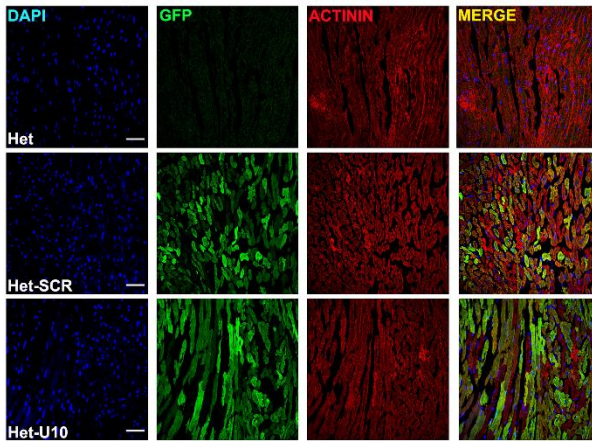
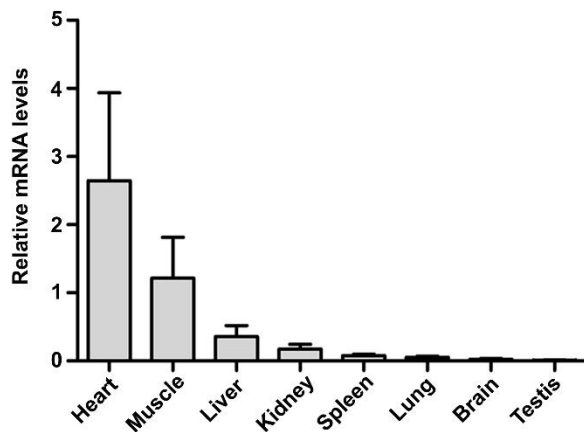
Mutant RYR2 mRNA :
5'- AACAGAAGCUGCUGAACUAUUUUGCU^UGCAACUUUUACAACAUGAGAAUGCUGGCC-3'

name	Seq 5'→3'
siRYR2-U5	UGC ^U UGCAACUUUUACAACAU
siRYR2-U6	UUGC ^U UGCAACUUUUACAACA
siRYR2-U7	UUUGC ^U UGCAACUUUUACAAC
siRYR2-U8	UUUUGC ^U UGCAACUUUUACAA
siRYR2-U9	AUUUUGC ^U UGCAACUUUUACA
siRYR2-U10	UAUUUUGC ^U UGCAACUUUUAC
siRYR2-U11	CUAUUUUGC ^U UGCAACUUUUA
siRYR2-U12	ACUAUUUUGC ^U UGCAACUUUU
siRYR2-U13	AACUAUUUUGC ^U UGCAACUUU
siRYR2-U14	GAACUAUUUUGC ^U UGCAACUU
siRYR2-U15	UGAACUAUUUUGC ^U UGCAACU
siRYR2-U16	CUGAACUAUUUUGC ^U UGCAAC
siRYR2-U17	GCUGAACUAUUUUGC ^U UGCAA

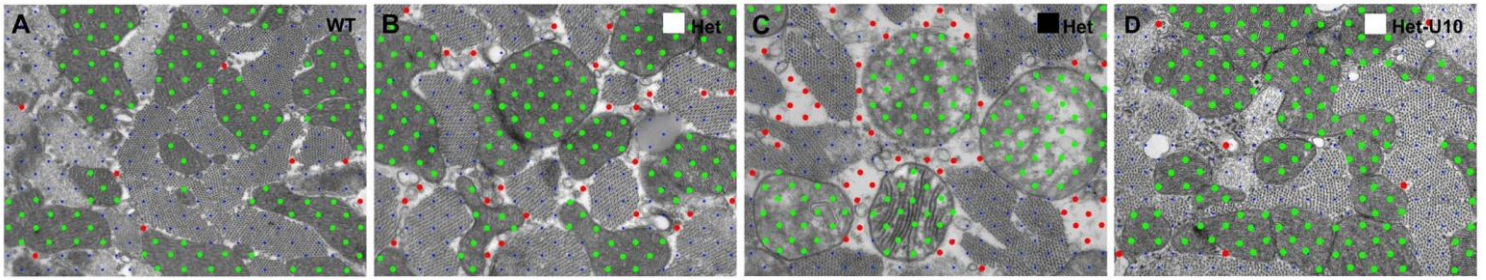
Online Figure I. Schematic drawing of siRNA duplexes and reporter alleles. **A**, Reporter alleles were constructed by inserting the region encompassing exon 91 to 96 of mutant and wild type *RYR2* cDNA downstream the reporter genes, *GFP* and *RFP* respectively, and fused with two different tags, 3XFLAG and 3XHA respectively, under CMV promoter (indicated by arrows). **B**, Portion of the wild type and mutant *RYR2* mRNAs and of the sense strand of the tested siRNA duplexes; mutation recognition site is in red.



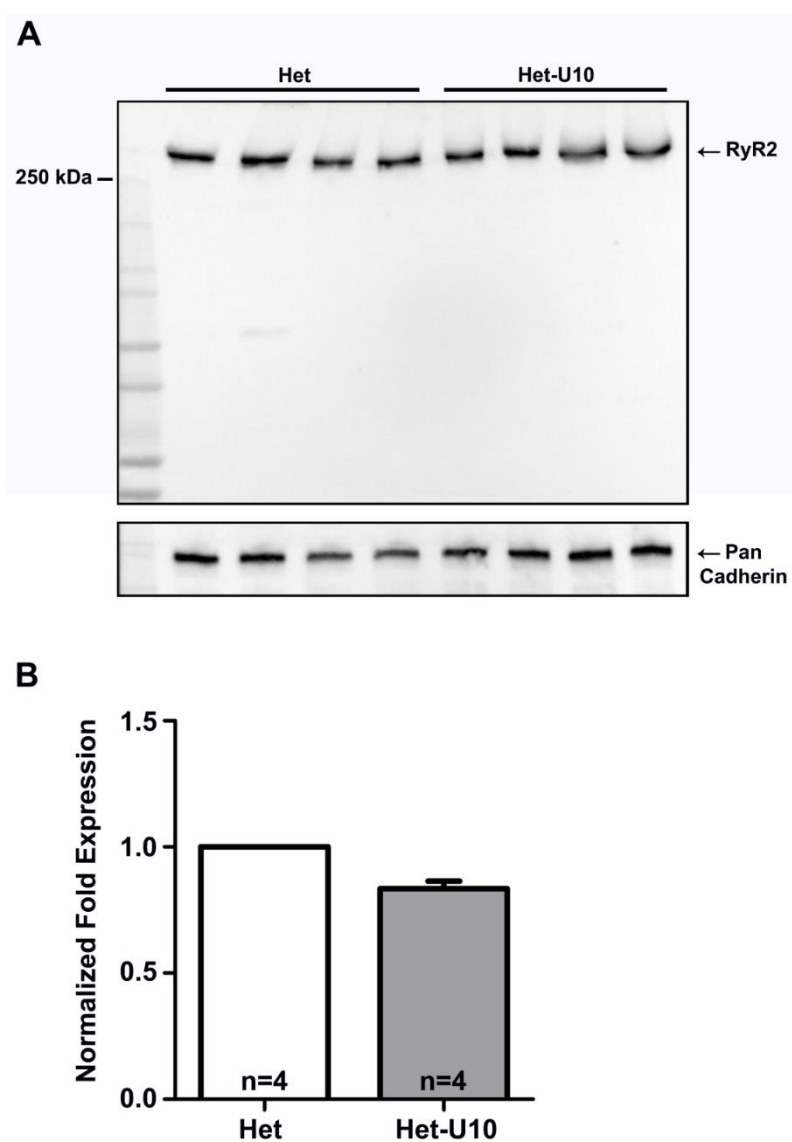
Online Figure II. Schematic drawing of miR YR2-U10 and miRNA-Scramble Expression Vectors. Cloning of annealed oligos, designed to replicate, when transcribed, sense and antisense strand of siR YR2-U10 (**A**) and siRNA-Scramble (**B**) into the miRNA Expression Vectors through a directional ligation.

A**B****C**

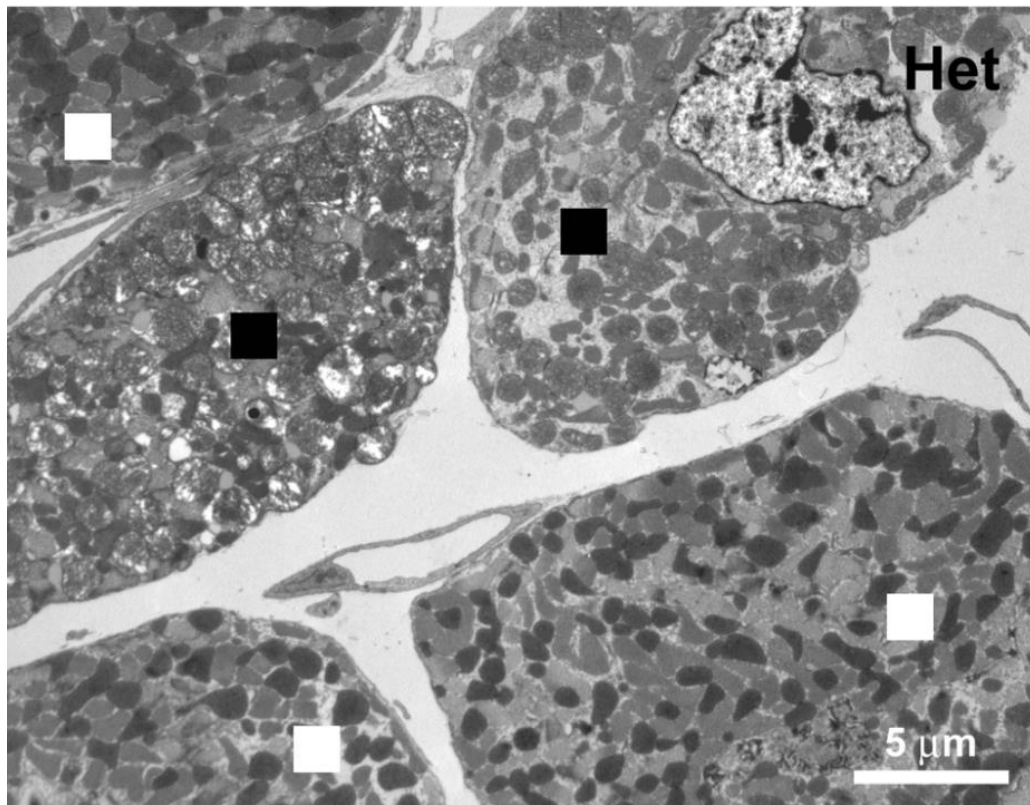
Online Figure III. Analysis of AAV9 vector transduction into murine cardiac myocytes. **A**, Estimation of percentage of infected GFP-positive cells (GFP) in comparison with total isolated cells (Phase Contrast). Scale bar=100 μ m. **B**, Immunofluorescence analysis with an anti-GFP antibody (green) in heart tissue section stained with α -actinin (red) to highlight the tissue distribution of AAV9-miR2-U10 and AAV9-miRNA-Scramble infection after 2 months in Het-SCR and Het-U10 mice. Het mice as negative control. Scale bar = 50 μ m. **C**, Real-time PCR quantification of GFP expression in AAV9-miR2-U10 infected RyR2^{R4496C/+} mice hearts and organs (n=3 each organ).



Online Figure IV. Method of ultrastructural cellular volume quantification. **A-D**, Representative images showing the method used to calculate the relative cell volume occupied by either mitochondria (green dots) or empty cytoplasmic space (red dots) in WT (**A**), Het (**B** and **C**, respectively in normal and severely altered cells) and Het-U10 (**D**) cardiomyocytes.



Online Figure V. Protein characterization of RyR2^{R4496C/+} mice treated with allele specific silencing. A, Immunoblotting of RyR2 and Pan Cadherin from total lysate of hearts derived from infected (Het-U10; n=4) and control mice (Het; n=4). **B,** RyR2 protein quantification normalized to Pan Cadherin levels.



Online Figure VI. Representative low magnification image of cardiac tissue from a Het sample. Cardiac cells were classified as normal (white square) or severely altered fibers (black square).

Supplemental Tables

Exp. Group	n° mice	Weight (g)	HR (bpm)	EDD mono (mm)	ESD mono (mm)	EF (%)
Het	14	23.1±3.9	413±42	4.4±0.38	3.3±0.41	50±7
Het-SCR	15	22.5±3.2	417±33	4.2±0.29	3.2±0.26	47±6
Het-U10	15	21.8±3.2	397±26	4.3±0.23	3.3±0.27	45±6
		<i>P</i> =0.630	<i>P</i> =0.228	<i>P</i> =0.305	<i>P</i> =0.527	<i>P</i> =0.108

Online Table I. Echocardiographic assessment of cardiac function in RyR2^{R4496C/+} mice treated with allele specific silencing and controls. Het, Het-SCR and Het-U10 mice were studied by echocardiography to evaluate left ventricular dimensions (EDD= end-diastolic diameter; ESD= end-systolic diameter) and cardiac function (HR= heart rate; EF= ejection fraction). No differences were observed in all the parameters among the three groups.

Exp. Group	No. of CRUs/ 20µm ²	No. of couplons/ 20µm ²	Average lenght of each couplon (nm)	jSR width (nm)
WT (3 hearts, 70 cardiomyocytes)	2.9±2.0	3.4±2.5	345±187	28.9±4.5
Het (3 hearts, 63 cardiomyocytes)	2.0±1.6 *	2.6±2.2 *	269±155	36.4±13.5 *
Het-U10 (3 hearts, 104 cardiomyocytes)	2.9±1.8 †	3.2±2.1 †	336±180 †	31.6±6.2 † ‡
Het-SCR (3 hearts, 62 cardiomyocytes)	1.1±1.2	1.6±1.8	263±142	35.1±10.8

Online Table II. Characterization of CRUs in WT and RyR2^{R4496C/+} mice treated with allele specific silencing.

Quantitative analysis of the number of CRUs in 20 µm², number of couplons in 20 µm², average length of each couplon (nm) and jSR width (nm) in WT, Het, Het-U10 and Het-SCR mice (WT vs Het: **P*< 0.05; Het-U10 vs Het: † *P*< 0.05; WT vs Het-U10: ‡ *P*< 0.05).

Boxes colored in green highlight fully recovered CRU parameters in heterozygous mice after U10 treatment (Definition of Fully Recovered=Het-U10 vs Het: † *P*< 0.05 and WT vs Het-U10: ‡ not significant)

Boxes colored in orange highlight Partially Recovered CRU parameters in heterozygous mice after U10 treatment (Definition of Partially Recovered=Het-U10 vs Het: † *P*< 0.05 while WT vs Het-U10: ‡ *P*<0.05)

Exp. Group	Cytoplasmic Volume/ Total Volume (%)	Mitochondrial Volume/ Total Volume (%)	SR Volume/ Total Volume (%)
WT (3 hearts, 65 cardiomyocytes)	2.0±2.2	34.7±6.1	3.0±1.3
Het (3 hearts, 78 cardiomyocytes)	11.7±8.5 *	28.4±6.4 *	2.2±1.2 *
Het-U10 (3 hearts, 111 cardiomyocytes)	1.4±2.4 †	37.2±6.7 †‡	3.2±1.4 †
Het-SCR (3 hearts, 62 cardiomyocytes)	11.5±8.5	29.6±8.2	1.9±1.4

Online Table III. Electron Microscopy analysis of ultrastructural abnormalities in WT and RyR2^{R4496C/+} mice treated with allele specific silencing.

Quantitative analysis of the relative volume occupied by cytoplasmic space, mitochondria and SR in WT, Het, Het-U10 and Het-SCR mice (WT vs Het: * $P < 0.05$; Het-U10 vs Het: † $P < 0.05$; WT vs Het-U10: ‡ $P < 0.05$).

Boxes colored in green highlight fully recovered mitochondrial parameters in heterozygous mice after U10 treatment (Definition of Fully Recovered= Het-U10 vs Het: † $P < 0.05$ and WT vs Het-U10: not significant)

Boxes colored in orange highlight Partially Recovered mitochondrial parameters in heterozygous mice after U10 treatment (Definition of Partially Recovered= Het-U10 vs Het: † $P < 0.05$ while WT vs Het-U10: $P < 0.05$)

Supplemental References

1. Cerrone M, Colombi B, Santoro M, Raffale di Barletta M, Scelsi M, Villani L, Napolitano C, Priori SG. Bidirectional Ventricular Tachycardia and Fibrillation Elicited in a Knock-In Mouse Model Carrier of a Mutation in the Cardiac Ryanodine Receptor (RyR2). *Circ Res*. 2005;96:e77–e82.
2. Cerrone M, Noujaim SF, Tolkacheva EG, Talkachou A, O’Connell R, Berenfeld O, Anumonwo J, Pandit S V., Vikstrom K, Napolitano C, Priori SG, Jalife J. Arrhythmogenic mechanisms in a mouse model of catecholaminergic polymorphic ventricular tachycardia. *Circ Res*. 2007;101:1039–1048.
3. Liu N, Ruan Y, Denegri M, Bachetti T, Li Y, Colombi B, Napolitano C, Coetzee WA, Priori SG. Calmodulin kinase II inhibition prevents arrhythmias in RyR2(R4496C+/-) mice with catecholaminergic polymorphic ventricular tachycardia. *J Mol Cell Cardiol*. 2011;50:214–222.
4. Loud A, Barany W, Pack B. QUANTITATIVE EVALUATION OF CYTOPLASMIC STRUCTURES IN ELECTRON MICROGRAPHS. *Lab Invest*. 1965;14:996–1008.
5. Mobley B a, Eisenberg BR. Sizes of components in frog skeletal muscle measured by methods of stereology. *J Gen Physiol*. 1975;66:31–45.

Legends for the Video files

Online video I. Transthoracic echocardiography in Het and Het-U10 mice.

The two videos show a parasternal long axis view of two months heterozygous mouse (A) and U10 mouse (B). The dimensions and systolic function are not different in the two animals (see Online Table I for details).